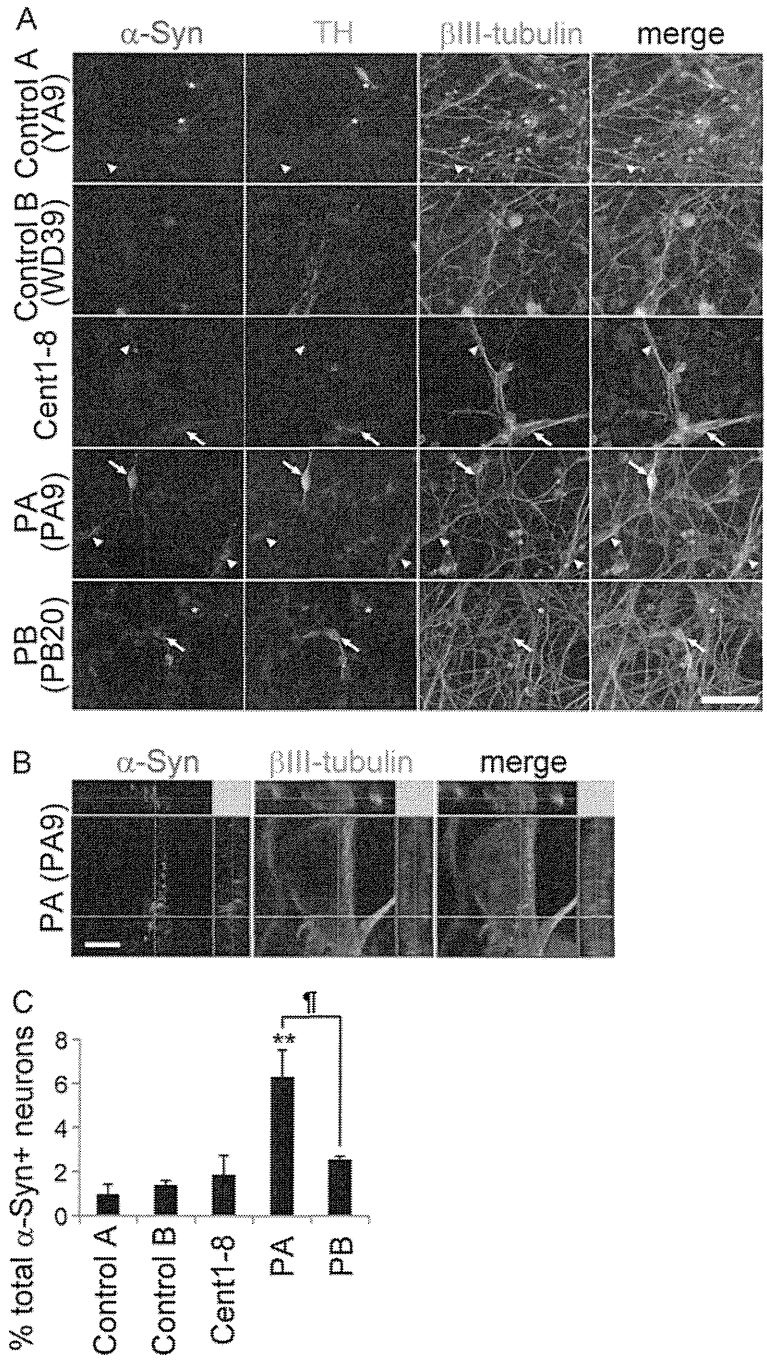

Figure 5 α-synuclein accumulation in PARK2 iPSC-derived neurons. (**A**–**C**) Triple labeling for α-synuclein (red), tyrosine hydroxylase (TH; cyan), and βIII-tubulin (green) along with Hoechst (blue) staining of control A (B7), control B (WD39), Cent1-8, and PARK2 (PA9 and PB20) iPSC-derived neurons. (**A**) Arrows indicate α-synuclein+/TH+/βIII-tubulin+ neurons; arrowheads indicate α-synuclein+/TH-/βIII-tubulin+ neurons. Note the presence of α-synuclein+/TH-/βIII-tubulin- non-neural cells (asterisks). (**B**) High magnification confocal projection image of an α-synuclein (magenta)/βIII-tubulin (green) double-positive PA9 iPSC-derived neuron. (**C**) The proportion of α-synuclein+/βIII-tubulin+ neurons relative to βIII-tubulin-positive neurons was significantly higher in PA (PA1, 9 and 22) iPSC-derived neurons than in control A (B7 and YA9), control B (WD39) and Cent1-8 iPSC-derived neurons. Scale bars: A, 50 μm; C, 5 μm. ** indicates $P < 0.01$; * and ¶ indicate $P < 0.05$ (Mann–Whitney *U*-test). Data represent the mean and SEM of at least three experiments for each group.

Sigma), NANOG (1:100, ReproCELL), OCT3/4 (1:200, Santa Cruz Biotechnology), SSEA-4 (1:200, Millipore), TRA-1-60 (1:200, Millipore), TH (1:100, Millipore), α-synuclein (1:500, Invitrogen), pα-synuclein (1:1000, Wako), cleaved-Caspase3 (1:500, Cell Signaling) and ComplexIII (C-III)-core I (1:200, Invitrogen). Cells were washed with PBS after incubation with the primary antibody, followed by incubation with an Alexa Fluor 488-, Alexa Fluor 555-, or Alexa Fluor 647-conjugated secondary antibody (1:500, Invitrogen). Images were obtained using Apotome (Zeiss) or LSM-710 confocal (Zeiss) microscopes.

PCR amplification of genomic DNA

Genomic DNA was purified from HDFs and iPSCs using a DNeasy kit (Qiagen). The PCR conditions used have been previously described [2,42].

Reverse transcription (RT)-PCR

RNA isolation and reverse transcription (RT)-PCR were performed as previously described [44]. The amount of cDNA was normalized to *β-actin* mRNA. Real-time RT-PCR was performed on a ABI PRISM Sequence detection System 7900HT (Applied BioSystems) using SYBR premix ExTaq (Takara). Primers for the detection of Oct4, the transgenes *Oct4-tg, Sox2-tg, Klf4-tg* and *c-Myc-tg*, and MAO-A, and -B have been previously described [10,15].

Teratoma assay

To assess teratoma formation, iPSCs were injected into the testis of 8-week-old NOD/SCID mice (OYG International) as previously described [14]. Eight weeks after transplantation, tumors were dissected and fixed with 4% PFA in PBS. Paraffin-embedded tissue was sectioned and stained with H&E. Images were obtained using a BZ-9000 (Keyence) microscope.

CGH array

Genomic DNA was restricted, labeled, and purified using the Agilent Oligo CGH Microarray Kit (Agilent Technologies) according to the manufacturer's protocol. Labeled genomic DNA was processed for hybridization on a 4x 180K microarray (Agilent Technologies). Processing was performed as instructed by the manufacturer. The genomic analysis was performed using Agilent Genomic Workbench ver. 6.0 software (Agilent Technologies).

Metabolism assays

Reduced GSH levels were measured according to the kit manufacturer's protocol (GSH-Glo Glutathione Assay; Promega). Chymotrypsin-like proteasome activity was measured using a Cell-Based Proteasome-Glo Assay according to the manufacturer's instructions (Promega). Briefly, neural cells (1.0×10^4) derived from neurospheres were seeded in triplicate into a white 96-well plate (Nunc). Prepared reagent (100 μl) was added to each well. After incubation for 10 min at RT, luminescence intensity was recorded. ROS levels were determined by measuring DCFH-DA fluorescence (Invitrogen). Briefly, neurons were incubated with 5 μM DCFH-DA and Hoechst (1:2000) for 30 min at 37°C, after which they were washed with PBS and then incubated in differentiation media. Fluorescence was measured by an In Cell Analyzer 2000 system (GE Healthcare Biosciences).

Protein analysis

Differentiated neurons were harvested in MAPK lysis buffer containing proteinase inhibitor, and protein concentrations were measured by BCA assay (Thermo Scientific). Samples were diluted to yield equivalent protein concentrations and then 4 μg was denatured by the addition of 4X sample buffer (Invitrogen) supplemented with β-mercaptoethanol followed by boiling. Samples (7 μl/lane) were loaded onto a 4–20% SDS-polyacrylamide gradient gel. Membranes were incubated in blocking solution with the indicated primary antibodies at 4°C overnight. Immunoreactive proteins were detected with horseradish peroxidase (HRP)-conjugated secondary antibodies and then visualized by chemiluminescence (Pierce, Rockford, IL, USA) according to the manufacturer's instructions. Quantification of band intensities was performed using an RAS4000 system. The primary antibodies used were anti-NQO1 (1:1000, Abcam), anti-NRF2 (1:1000, Santa Cruz Biotechnology) and β-actin (1:5000, Cell Signaling).

CCCP and Baf A_1 treatments

Neurons were cultured with 30 μM CCCP (Sigma-Aldrich) or DMSO, with or without 5 μM Baf A_1 (Sigma-Aldrich), for 48 h. The cells were then fixed and stained for βIII-tubulin and C-III Core I, and counterstained with Hoechst. To quantify the IMM area of the neurons, the cytoplasmic area was extracted as shown in Figure 3C. The C-III Core I-positive signals within the extracted area were then converted to gray-scale and digitized. The IMM area was quantified from the digitized values using Image J software.

Tetramethylrhodamine ethyl ester (TMRE) staining

iPSC-derived neurons were incubated with 1nM TMRE (Invitrogen) for 15 min at 37°C and then observed under an Olympus IX81 microscope.

Electron microscopy

Cells were fixed with 2% glutaraldehyde/2% PFA in 0.1 M phosphate buffer (PB) (pH7.2), post-fixed with 1% OsO4 in 0.1 M PB (pH 7.2), blocked and stained with a 2% aqueous solution of uranyl acetate, dehydrated with a graded series of ethanol, and then embedded in Epon 812 (TAAB). Coverslips were detached and the embedded samples were placed under a stereomicroscope to identify the cells of

interest. Ultrathin sections were cut with a Leica UC6 or UC7 ultramicrotome (Leica Microsystems) and then stained with uranyl acetate and lead citrate. Samples were observed with a Hitachi H7100 or HT7700 electron microscope.

Morphometry

Morphometric analysis was used to measure the volume density of mitochondria in the neuronal perikarya as previously described [45]. Briefly, electron micrographs of neurons (n = 20, 23, 41, and 44 for control A (B7), control B (WD39), PA9 and PB2, respectively) were obtained at a magnification of ×7000. After enlarging to three times the original magnification, point-counting was carried out to determine the volume density using a double-lattice test system with 1.5 cm spacing. Mitochondria were classified as normal, abnormal, or undetermined. The abnormal mitochondria were defined as those with irregularly arranged cristae, or with a high electron-dense matrix. The volume density (Vv) of each type of mitochondrion was expressed as percent volume according to the following formula: Vv = (Pi/Pt) × 100 (%), where Pi is the number of points falling on each mitochondrial structure and Pt is the number of points falling on the neuronal perikarya.

Immunohistochemical analysis of autopsied brain tissue

The ethical committee of the Kitasato University School of Medicine and Juntendo University School of Medicine reviewed and approved the protocol for analysis of autopsied brain tissue. Patients and control subjects were informed of the study and gave written informed consent. Brain tissue from patient PA was obtained following her death at age 72; brain tissue from the father of patient PB was obtained when he died at age 70 [46]. Tissue was fixed with 10% formalin and then embedded in paraffin. Midbrain sections (6 μm thick) were cut, deparaffinized with xylene, and then rehydrated in ethanol. After being boiled and treated with H_2O_2, sections were subjected to immunofluorescence staining with antibodies to the following proteins: α-synuclein (1:500, Invitrogen), pα-synuclein (1:1000, Wako), and TH (1:1000, Calbiochem). After washing with PBS, sections were incubated with a biotinylated secondary antibody (1:500; Vector Laboratories Inc.) at RT for 1 hr followed by incubation with an avidin-biotin peroxidase complex (Vector Laboratories Inc.) for 1 hr. Immunoreactive proteins were visualized using 3,3-diaminobenzidine (DAB; Wako Pure Chemical Industries) and nuclear fast red staining. For immunofluorescence, FITC-conjugated and Cy3-conjugated secondary antibodies (1:500; Jackson Immunoresearch Laboratories) were used. Images were obtained using a BIOREVO (Keyence) and a confocal laser-scanning LSM710 (Zeiss) microscope.

Statistical analysis

Values represent the mean ± SEM. The Mann–Whitney *U*-test was used to evaluate differences between groups. A P value of < 0.05 was considered significant.

Additional files

Additional file 1: Genetic studies of family. (A) An arrow indicates PA patient. (B) An arrow indicates PB patient. Filled circles and squares, women and men with PARK2 mutation; Open circles and squares, normal women and men; Diamond shapes, family members whose DNA samples were not analyzed. Symbols with lines through them represent the deceased.

Additional file 2: Characterization of control and PARK2 iPSCs. (A) Control A (YA9), Control B (WD39), PA (PA9), and PB (PB2) iPSCs expressed the pluripotency markers SSEA4 (red) and TRA1-60 (green). Scale bar, 100 μm. (B) iPSCs established from patients PA (PA1, PA22) and PB (PB1, PB18, and PB20) were positive for the pluripotency markers Nanog (red), Oct4 (green), SSEA4 (red), and TRA1-60 (green). Scale bars: phase images, 200 μm; immunofluorescence images, 100 μm. (C) Levels of endogenous *Oct4* mRNA in the generated iPSCs were similar to those in KhES1 cells, a human embryonic stem cell (hESC) line [42]. Expression levels were normalized to that of KhES1 (set as 1). (D) Cont A (YA9), Cont B (WD39), PA (PA1, 9 and 22), and PB (PB1, 2, 18 and 20) iPSCs gave rise to teratomas with all three germ layers, confirming pluripotency. Scale bar, 100 μm. (E) Silencing of transgenes in control and PARK2 iPSC clones. Expression levels were normalized to the positive control of fibroblasts in cultures assayed 6 days after retroviral infection (= 100). Cont A, Control A; Cont B, Control B.

Additional file 3: Confirmation of *parkin* deletions and genomic stability of PARK2 iPSCs using comparative genomic hybridization (CGH) microarray analysis. (A) Exons 2–4 were deleted in the PA9 and PA22 iPSC lines. Exons 6 and 7 were deleted in the PB2, 18, and 20 iPSC lines. (B) Copy number profiles of whole chromosomes in PARK2 iPSCs assessed by CGH microarray analysis revealed that no genomic aberrations were introduced during the process of establishing PARK2 iPSCs.

Additional file 4: Expression level of MAO-A and -B showed no difference among Control and PARK2 iPSC-derived neurons. (A,B) qRT-PCR measurement of MAO-A and -B transcripts in PARK2 (PA (1, 9 and 22) and PB (1, 2 and 20)) iPSC-derived neurons showed no difference compared to those in Cont A (B7 and YA9). ContA; Control A, ContB; Control B.

Additional file 5: Healthy mitochondria in PARK2 fibroblasts and iPSCs. (A, B) Electron micrographs of fibroblasts (upper panels) and iPSCs (lower panels) from Control (Cont A and Cont B) and PARK2 patients (PA and PB). Mitochondria in the fibroblasts and iPSCs from both groups showed long, cylindrical profiles with well-organized cristae, and the electron density of the matrix was relatively low (asterisks). Scale bar, 0.25 μm. Cont A, Control A; Cont B, Control B. (C) Fibroblasts were treated with 30μM CCCP or DMSO for 48 h, followed by staining for CIII corel (magenta) to label the internal mitochondrial membrane (IMM) and counterstaining with Hoechst (Ho, blue). Mitochondrial size decreased after CCCP treatment in both Control (Cont A and Cont B) and PARK2 (PA and PB) fibroblasts. Scale bar, 20 μm. (D) iPSCs were treated with 30 μM CCCP or DMSO for 48 h and then stained for CIII corel (magenta) to label IMM, Oct4 (blue) to label iPSCs, and Hoechst (Ho, white). Mitochondrial size in Control (Cont A (B7), Cont B (WD39)), and PARK2 (PA9 and PB2) iPSCs decreased after CCCP treatment. Scale bar, 20 μm (E) CCCP/DMSO ratios in Control (Cont A (B7, YA9), Cont B (WD39)), and PARK2 (PA9 and 22 and PB2 and 20) iPSCs (Mann Whitney *U*-test). Data represent the mean and SEM ($n > 3$ for each group).

Additional file 6: Mitochondrial membrane potential after CCCP treatment in control and PARK2 iPSC-derived neurons. (A) iPSC-derived neurons were treated with 30 μM CCCP or DMSO for 48 h, after which they were stained for the mitochondrial membrane potential marker, TMRE. The intensity of TMRE (yellow) was clearly reduced in

control (Cont A (B7), Cont B (WD39)), and PARK2 (PA9 and PB2) iPSC-derived neurons. Scale bar, 50 μm.

Additional file 7: Confirmation of *parkin* deletions carried by the father of patient PB. (A) Deletion of exons 6 and 7 was confirmed in blood samples from PB and the father of PB by PCR.

Additional file 8: α-Synuclein signals are not seen in PARK2 iPSCs. (A) Quantitative genomic PCR analysis for SNCA exons 1 and 4 demonstrated a normal copy number in PARK2 (PA1, 9 and 22, and PB1, 2, 18 and 20) iPSCs. The copy number was the same as that observed for Cont A (B7 and YA9) and Cont B (WD39). The *SNCA* gene copy number was normalized to β-globin *(HBB)* and β2-microglobulin *(B2MG)*. (B) iPSCs were stained for α-synuclein (red), Oct4 (green; to label iPSCs) and Hoechst (blue). No α-synuclein signals were observed in Cont A (B7 and YA9), Cont B (WD39), or PARK2 (PA9 and 22, PB2 and 20) iPSCs. Scale bar, 50 μm.

Competing interests
The authors declare that they have no competing interests.

Authors' contributions
YI, YO, WA, and HO conceived and designed the experiments. YI performed most of the experiments, analyzed data, and wrote the manuscript. YO, and HO edited the manuscript. YO developed the quality control system, neural differentiation method for the iPSCs and performed CGH microarray data analysis. WA generated the WD39 iPSCs. NK, KH, MS and AN performed western blotting analysis. TN performed some parts of *in vitro* culture assay. SS, MF, YM, HM and NH examined and recruited PARK2 patients. TK, MO, and MA performed biopsies and established the skin fibroblasts. AH, TS, TH and MS performed preliminary experiments for the metabolome analysis. TY, DI, AK and NS provided cent8-1 iPSCs. YI and NM designed the CCCP treatment experiment. MK and YU performed the electron microscopic analysis. HH, MT, HM and NH performed the histopathological studies of the postmortem brain of PA. All authors read and approved the final manuscript.

Acknowledgments
We would like to thank S. Yamanaka (CiRA) for the 201B7 iPSCs; N. Nakatsuji (Kyoto University) for the KhES cells; N. Izawa, S. Banno, Y. Matsuzaki, M. Fujiwara, Y. Nagahata, N. Hirose (Keio University), C. Kishi (Tokyo Medical and Dental University), M. Ogino, S. Miyakawa, (Kitasato University) and G. Takata (GE Healthcare Biosciences) for technical assistance and suggestions. This work was supported by the Project for the Realization of Regenerative Medicine and Support for the Core Institutes for iPS cell research from the Japanese Ministry of Education, Culture, Sports, Science and Technology (MEXT) to H.O., Exploratory Research for Advanced Technology (ERATO), Suematsu Gas Biology Project from Japan Science and Technology Agency (JST) to M.S., a Grant-in-Aid from the Japan Society for the Promotion of Science (JSPS) to W.A. and Y.O., the Keio Kanrinmaru Project and a Grant-in-Aid for Scientific Research on Innovative Areas to Y.O., a Grant-in-Aid for Scientific Research on Innovative Areas (Comprehensive Brain Science Network) from the MEXT to Y. O. and Y. I., a Grant-in-Aid for Encouragement of Young Medical Scientists from Keio University and the Japan Society for the Promotion of Science Fellows to Y.I., and a Grant-in-Aid for the Global COE Program at Keio University.

Author details
[1]Department of Physiology, Keio University School of Medicine, 35 Shinanomachi, Shinjuku-ku, Tokyo 160-8582, Japan. [2]Kanrinmaru Project, Keio University School of Medicine, Tokyo, Japan. [3]Department of Cell Biology and Neuroscience, Juntendo University Graduate School of Medicine, Tokyo, Japan. [4]Department of Neurology, Kitasato University School of Medicine, Kanagawa, Japan. [5]Department of Dermatology, Keio University School of Medicine, Tokyo, Japan. [6]Department of Neurology, Juntendo University School of Medicine, Tokyo, Japan. [7]Research Institute for Diseases of Old Age, Graduate School of Medicine, Juntendo University, Tokyo, Japan. [8]Institute for Advanced Biosciences, Keio University, Yamagata, Japan. [9]Department of Biochemistry, Keio University School of Medicine, Tokyo, Japan. [10]Department of Neurology, Keio University School of Medicine, Tokyo, Japan. [11]Advanced Science Research Laboratories, Pharmaceutical Research Division, Takeda Pharmaceutical Company Limited, Kanagawa, Japan. [12]Department of Neuro-Regenerative Medicine, Kitasato University School of Medicine, Kanagawa, Japan. [13]Department of Physiology and Cell Biology, Tokyo Medical and Dental University, Tokyo, Japan. [14]Department of Neurology, Osaka University Graduate School of Medicine, Osaka, Japan.

Received: 19 September 2012 Accepted: 2 October 2012
Published: 6 October 2012

References
1. Farrer MJ: **Genetics of Parkinson disease: paradigm shifts and future prospects.** *Nature reviews* 2006, **7**:306–318.
2. Kitada T, Asakawa S, Hattori N, Matsumine H, Yamamura Y, Minoshima S, Yokochi M, Mizuno Y, Shimizu N: **Mutations in the parkin gene cause autosomal recessive juvenile parkinsonism.** *Nature* 1998, **392**:605–608.
3. Shimura H, Hattori N, Kubo S, Mizuno Y, Asakawa S, Minoshima S, Shimizu N, Iwai K, Chiba T, Tanaka K, Suzuki T: **Familial Parkinson disease gene product, parkin, is a ubiquitin-protein ligase.** *Nat Genet* 2000, **25**:302–305.
4. Whitworth AJ, Pallanck LJ: **The PINK1/Parkin pathway: a mitochondrial quality control system?** *J Bioenerg Biomembr* 2009, **41**:499–503.
5. Youle RJ, Narendra DP: **Mechanisms of mitophagy.** *Nat Rev Mol Cell Biol* 2011, **12**:9–14.
6. Goldberg MS, Fleming SM, Palacino JJ, Cepeda C, Lam HA, Bhatnagar A, Meloni EG, Wu N, Ackerson LC, Klapstein GJ, *et al*: **Parkin-deficient mice exhibit nigrostriatal deficits but not loss of dopaminergic neurons.** *J Biol Chem* 2003, **278**:43628–43635.
7. Palacino JJ, Sagi D, Goldberg MS, Krauss S, Motz C, Wacker M, Klose J, Shen J: **Mitochondrial dysfunction and oxidative damage in parkin-deficient mice.** *J Biol Chem* 2004, **279**:18614–18622.
8. Perez FA, Palmiter RD: **Parkin-deficient mice are not a robust model of parkinsonism.** *Proc Natl Acad Sci USA* 2005, **102**:2174–2179.
9. Sato S, Chiba T, Nishiyama S, Kakiuchi T, Tsukada H, Hatano T, Fukuda T, Yasoshima Y, Kai N, Kobayashi K, *et al*: **Decline of striatal dopamine release in parkin-deficient mice shown by ex vivo autoradiography.** *J Neurosci Res* 2006, **84**:1350–1357.
10. Jiang H, Ren Y, Yuen EY, Zhong P, Ghaedi M, Hu Z, Azabdaftari G, Nakaso K, Yan Z, Feng J: **Parkin controls dopamine utilization in human midbrain dopaminergic neurons derived from induced pluripotent stem cells.** *Nat Commun* 2012, **3**:668.
11. Mattis VB, Svendsen CN: **Induced pluripotent stem cells: a new revolution for clinical neurology?** *Lancet Neurol* 2011, **10**:383–394.
12. Farrer M, Chan P, Chen R, Tan L, Lincoln S, Hernandez D, Forno L, Gwinn-Hardy K, Petrucelli L, Hussey J, *et al*: **Lewy bodies and parkinsonism in families with parkin mutations.** *Ann Neurol* 2001, **50**:293–300.
13. Savitt JM, Dawson VL, Dawson TM: **Diagnosis and treatment of Parkinson disease: molecules to medicine.** *J Clin Invest* 2006, **116**:1744–1754.
14. Ohta S, Imaizumi Y, Okada Y, Akamatsu W, Kuwahara R, Ohyama M, Amagai M, Matsuzaki Y, Yamanaka S, Okano H, Kawakami Y: **Generation of human melanocytes from induced pluripotent stem cells.** *PLoS One* 2011, **6**:e16182.
15. Takahashi K, Tanabe K, Ohnuki M, Narita M, Ichisaka T, Tomoda K, Yamanaka S: **Induction of pluripotent stem cells from adult human fibroblasts by defined factors.** *Cell* 2007, **131**:861–872.
16. Matigian N, Abrahamsen G, Sutharsan R, Cook AL, Vitale AM, Nouwens A, Bellette B, An J, Anderson M, Beckhouse AG, *et al*: **Disease-specific, neurosphere-derived cells as models for brain disorders.** *Dis Model Mech* 2010, **3**:785–798.
17. Nguyen HN, Byers B, Cord B, Shcheglovitov A, Byrne J, Gujar P, Kee K, Schule B, Dolmetsch RE, Langston W, *et al*: **LRRK2 mutant iPSC-derived DA neurons demonstrate increased susceptibility to oxidative stress.** *Cell Stem Cell* 2011, **8**:267–280.
18. Sies H: **Glutathione and its role in cellular functions.** *Free Radic Biol Med* 1999, **27**:916–921.
19. Williamson TP, Johnson DA, Johnson JA: **Activation of the Nrf2-ARE pathway by siRNA knockdown of Keap1 reduces oxidative stress and provides partial protection from MPTP-mediated neurotoxicity.** *Neurotoxicology* 2012, **33**:272–279.
20. Ramsey CP, Glass CA, Montgomery MB, Lindl KA, Ritson GP, Chia LA, Hamilton RL, Chu CT, Jordan-Sciutto KL: **Expression of Nrf2 in neurodegenerative diseases.** *J Neuropathol Exp Neurol* 2007, **66**:75–85.
21. Tufekci KU, Civi Bayin E, Genc S, Genc K: **The Nrf2/ARE Pathway: a promising target to counteract mitochondrial dysfunction in parkinson's disease.** *Parkinsons Dis* 2011, **2011**:314082.

22. Fukae J, Mizuno Y, Hattori N: **Mitochondrial dysfunction in Parkinson's disease.** *Mitochondrion* 2007, **7**:58–62.
23. Schapira AH: **Mitochondrial dysfunction in neurodegenerative disorders.** *Biochim Biophys Acta* 1998, **1366**:225–233.
24. Greene JC, Whitworth AJ, Kuo I, Andrews LA, Feany MB, Pallanck LJ: **Mitochondrial pathology and apoptotic muscle degeneration in Drosophila parkin mutants.** *Proc Natl Acad Sci USA* 2003, **100**:4078–4083.
25. Mortiboys H, Thomas KJ, Koopman WJ, Klaffke S, Abou-Sleiman P, Olpin S, Wood NW, Willems PH, Smeitink JA, Cookson MR, Bandmann O: **Mitochondrial function and morphology are impaired in parkin-mutant fibroblasts.** *Ann Neurol* 2008, **64**:555–565.
26. Matsuda N, Sato S, Shiba K, Okatsu K, Saisho K, Gautier CA, Sou YS, Saiki S, Kawajiri S, Sato F, *et al*: **PINK1 stabilized by mitochondrial depolarization recruits Parkin to damaged mitochondria and activates latent Parkin for mitophagy.** *J Cell Biol* 2010, **189**:211–221.
27. Narendra D, Tanaka A, Suen DF, Youle RJ: **Parkin is recruited selectively to impaired mitochondria and promotes their autophagy.** *J Cell Biol* 2008, **183**:795–803.
28. Tanaka A: **Parkin-mediated selective mitochondrial autophagy, mitophagy: Parkin purges damaged organelles from the vital mitochondrial network.** *FEBS Lett* 2010, **584**:1386–1392.
29. Yoshii SR, Kishi C, Ishihara N, Mizushima N: **Parkin mediates proteasome-dependent protein degradation and rupture of the outer mitochondrial membrane.** *J Biol Chem* 2011, **286**:19630–19640.
30. Seibler P, Graziotto J, Jeong H, Simunovic F, Klein C, Krainc D: **Mitochondrial Parkin recruitment is impaired in neurons derived from mutant PINK1 induced pluripotent stem cells.** *J Neurosci* 2011, **31**:5970–5976.
31. Shults CW: **Lewy bodies.** *Proc Natl Acad Sci USA* 2006, **103**:1661–1668.
32. Pramstaller PP, Schlossmacher MG, Jacques TS, Scaravilli F, Eskelson C, Pepivani I, Hedrich K, Adel S, Gonzales-McNeal M, Hilker R, *et al*: **Lewy body Parkinson's disease in a large pedigree with 77 Parkin mutation carriers.** *Ann Neurol* 2005, **58**:411–422.
33. Sasaki S, Shirata A, Yamane K, Iwata M: **Parkin-positive autosomal recessive juvenile Parkinsonism with alpha-synuclein-positive inclusions.** *Neurology* 2004, **63**:678–682.
34. Schlossmacher MG, Frosch MP, Gai WP, Medina M, Sharma N, Forno L, Ochiishi T, Shimura H, Sharon R, Hattori N, *et al*: **Parkin localizes to the Lewy bodies of Parkinson disease and dementia with Lewy bodies.** *Am J Pathol* 2002, **160**:1655–1667.
35. Chung KK, Zhang Y, Lim KL, Tanaka Y, Huang H, Gao J, Ross CA, Dawson VL, Dawson TM: **Parkin ubiquitinates the alpha-synuclein-interacting protein, synphilin-1: implications for Lewy-body formation in Parkinson disease.** *Nat Med* 2001, **7**:1144–1150.
36. Petrucelli L, O'Farrell C, Lockhart PJ, Baptista M, Kehoe K, Vink L, Choi P, Wolozin B, Farrer M, Hardy J, Cookson MR: **Parkin protects against the toxicity associated with mutant alpha-synuclein: proteasome dysfunction selectively affects catecholaminergic neurons.** *Neuron* 2002, **36**:1007–1019.
37. Shimura H, Schlossmacher MG, Hattori N, Frosch MP, Trockenbacher A, Schneider R, Mizuno Y, Kosik KS, Selkoe DJ: **Ubiquitination of a new form of alpha-synuclein by parkin from human brain: implications for Parkinson's disease.** *Science (New York, NY)* 2001, **293**:263–269.
38. Yagi T, Kosakai A, Ito D, Okada Y, Akamatsu W, Nihei Y, Nabetani A, Ishikawa F, Arai Y, Hirose N, *et al*: **Establishment of induced pluripotent stem cells from centenarians for neurodegenerative disease research.** *PLoS One* 2012, **7**:e41572.
39. Hargus G, Cooper O, Deleidi M, Levy A, Lee K, Marlow E, Yow A, Soldner F, Hockemeyer D, Hallett PJ, *et al*: **Differentiated Parkinson patient-derived induced pluripotent stem cells grow in the adult rodent brain and reduce motor asymmetry in Parkinsonian rats.** *Proc Natl Acad Sci USA* 2010, **107**:15921–15926.
40. Park IH, Arora N, Huo H, Maherali N, Ahfeldt T, Shimamura A, Lensch MW, Cowan C, Hochedlinger K, Daley GQ: **Disease-Specific Induced Pluripotent Stem Cells.** *Cell* 2008, .
41. Soldner F, Hockemeyer D, Beard C, Gao Q, Bell GW, Cook EG, Hargus G, Blak A, Cooper O, Mitalipova M, *et al*: **Parkinson's disease patient-derived induced pluripotent stem cells free of viral reprogramming factors.** *Cell* 2009, **136**:964–977.
42. Devine MJ, Ryten M, Vodicka P, Thomson AJ, Burdon T, Houlden H, Cavaleri F, Nagano M, Drummond NJ, Taanman JW, *et al*: **Parkinson's disease induced pluripotent stem cells with triplication of the alpha-synuclein locus.** *Nat Commun* 2011, **2**:440.
43. Suemori H, Yasuchika K, Hasegawa K, Fujioka T, Tsuneyoshi N, Nakatsuji N: **Efficient establishment of human embryonic stem cell lines and long-term maintenance with stable karyotype by enzymatic bulk passage.** *Biochem Biophys Res Commun* 2006, **345**:926–932.
44. Okada Y, Matsumoto A, Shimazaki T, Enoki R, Koizumi A, Ishii S, Itoyama Y, Sobue G, Okano H: **Spatiotemporal recapitulation of central nervous system development by murine embryonic stem cell-derived neural stem/progenitor cells.** *Stem cells (Dayton, Ohio)* 2008, **26**:3086–3098.
45. Koike M, Shibata M, Waguri S, Yoshimura K, Tanida I, Kominami E, Gotow T, Peters C, von Figura K, Mizushima N, *et al*: **Participation of autophagy in storage of lysosomes in neurons from mouse models of neuronal ceroid-lipofuscinoses (Batten disease).** *Am J Pathol* 2005, **167**:1713–1728.
46. Mitsui J, Takahashi Y, Goto J, Tomiyama H, Ishikawa S, Yoshino H, Minami N, Smith DI, Lesage S, Aburatani H, *et al*: **Mechanisms of genomic instabilities underlying two common fragile-site-associated loci, PARK2 and DMD, in germ cell and cancer cell lines.** *Am J Hum Genet* 2010, **87**:75–89.

doi:10.1186/1756-6606-5-35
Cite this article as: Imaizumi *et al.*: Mitochondrial dysfunction associated with increased oxidative stress and α-synuclein accumulation in PARK2 iPSC-derived neurons and postmortem brain tissue. *Molecular Brain* 2012 5:35.

FEBS Letters xxx (2013) xxx–xxx

FEBS Letters

journal homepage: www.FEBSLetters.org

ATP13A2 deficiency induces a decrease in cathepsin D activity, fingerprint-like inclusion body formation, and selective degeneration of dopaminergic neurons

Q1 Hideaki Matsui [a,g,1,2], Fumiaki Sato [b,g,1,3], Shigeto Sato [b,g], Masato Koike [f], Yosuke Taruno [a,g], Shinji Saiki [b,g], Manabu Funayama [d,g], Hidefumi Ito [a,g], Yoshihito Taniguchi [c,g,4], Norihito Uemura [a,g], Atsushi Toyoda [e,6], Yoshiyuki Sakaki [e,5], Shunichi Takeda [c,g], Yasuo Uchiyama [f], Nobutaka Hattori [b,g,*], Ryosuke Takahashi [a,g,*]

[a] Department of Neurology, Kyoto University Graduate School of Medicine, Kyoto 606-8507, Japan
[b] Department of Neurology, Juntendo University, School of Medicine, 2-1-1 Hongo, Bunkyo-ku, Tokyo 113-8421, Japan
[c] Department of Radiation Genetics, Kyoto University Graduate School of Medicine, Kyoto 606-8501, Japan
[d] Research Institute for Diseases of Old Age, Juntendo University, School of Medicine, 2-1-1 Hongo, Bunkyo-ku, Tokyo 113-8421, Japan
[e] RIKEN Genomic Sciences Center, Yokohama 230-0045, Japan
[f] Department of Cell Biology and Neuroscience, Juntendo University, School of Medicine, 2-1-1 Hongo, Bunkyo-ku, Tokyo 113-8421, Japan
[g] Core Research for Evolutional Science and Technology (CREST), Japan Science and Technology Agency, Kawaguchi 332-0012, Japan

ARTICLE INFO

Article history:
Received 5 January 2013
Revised 22 February 2013
Accepted 25 February 2013
Available online xxxx

Edited by Barry Halliwell

Q2 *Keywords:*
Parkinson's disease
Medaka fish
ATP13A2
Lysosome

ABSTRACT

Kufor-Rakeb syndrome (KRS) was originally described as an autosomal recessive form of early-onset parkinsonism with pyramidal degeneration and dementia. *ATP13A2* was identified as the causative gene in KRS. *ATP13A2* encodes the ATP13A2 protein, which is a lysosomal type5 P-type ATPase, and ATP13A2 mutations are linked to autosomal recessive familial parkinsonism.

Here, we report that normal ATP13A2 localizes in the lysosome, whereas disease-associated variants remain in the endoplasmic reticulum. Cathepsin D activity was decreased in ATP13A2-knockdown cells that displayed lysosome-like bodies characterized by fingerprint-like structures. Furthermore, an atp13a2 mutation in medaka fish resulted in dopaminergic neuronal death, decreased cathepsin D activity, and fingerprint-like structures in the brain. Based on these results, lysosome abnormality is very likely to be the primary cause of KRS/PARK9.

1. Introduction

Parkinson's disease (PD) is one of the most common movement disorders, and it is caused by loss of dopaminergic neurons. The molecular mechanisms underlying neuronal degeneration in PD remain unknown; however, it is now clear that genetic factors heavily contribute to the pathogenesis of this disease [1]. In approximately 10% of patients with clinical features of PD, the disease state has a strict familial etiology.

PARK9-linked PD is an autosomal recessive early-onset disorder that is characterized by levodopa-responsive parkinsonism, supranuclear gaze palsy, pyramidal signs, and dementia; this condition is also called Kufor-Rakeb syndrome (KRS), being named for a consanguineous Jordanian family containing four members with this disorder [2]. Recently, *ATP13A2* was identified as the causative gene for KRS/PARK9. The *ATP13A2* gene comprises 29 exons that encode a lysosomal type 5 P-type ATPase with 10 transmembrane domains [3]. Thus far, eight mutations have been reported in just five families and in two additional unrelated patients, and no neuropathological examination of an autopsy case has been documented [3–8]. The function of the ATP13A2 protein remains largely unknown, but it is supposed that ATP13A2 might participate in autophagic protein degradation via the lysosomal pathway [9].

Here, we established and analyzed a cell culture model of ATP13A2 knockdown and Atp13a2 mutant medaka fish to elucidate the mechanisms underlying PARK9-associated pathology.

* Corresponding authors.
E-mail addresses: nhattori@juntendo.ac.jp (N. Hattori), ryosuket@kuhp.kyoto-u.ac.jp (R. Takahashi).

[1] These authors contributed equally to this work.

[2] Current address: Department of Cell Physiology, Zoological Institute, Technical University Braunschweig, Spielmannstrasse 8, Braunschweig 38106, Germany.

[3] Current address: Department of Clinical Chemistry, Hoshi University School of Pharmacy and Pharmaceutical Sciences, 2-4-41 Ebara, Shinagawa-ku, Tokyo 142-8501, Japan.

[4] Current address: Department of Preventive Medicine and Public Health, School of Medicine, Keio University, 35, Shinano-cho, Shinjuku-ku, Tokyo 160-8582, Japan.

[5] Current address: Toyohashi University of Technology, 1-1, Hibarigaoka, Tenpaku-cho, Toyohashi, Aichi 441-8580, Japan.

[6] Current address: Comparative Genomics Laboratory, National Institute of Genetics, Yata 1111, Mishima, Shizuoka 411-8540, Japan.

0014-5793/$36.00 © 2013 Published by Elsevier B.V. on behalf of the Federation of European Biochemical Societies.
http://dx.doi.org/10.1016/j.febslet.2013.02.046

Both the cultured cells and the mutant fish exhibited decreased cathepsin D enzymatic activity, fingerprint-like inclusion body formation, and neuronal death. These findings indicated that abnormalities in lysosome function are the primary defect in KRS/PARK9.

2. Results

2.1. Wild-type ATP13A2 localizes to the lysosome, but some disease-relevant variants localize to the endoplasmic reticulum

To investigate the subcellular localization of ATP13A2, we used an anti-V5 antibody and antibodies that recognize several markers of intracellular organelles to double label SH-SY5Y cells that stably expressed wild-type ATP13A2 fused to the V5 epitope (WT-V5). The WT-V5 signal largely colocalized with the signal of cathepsin D, a lysosomal aspartic protease (Fig. 1A and S1). Additionally, WT-V5 partially overlapped with makers of the Golgi apparatus (GM130), the late endosome (Rab7) and the autophagosome (LC3B), but not with the markers of the endoplasmic reticulum (ER) (GRP78), the mitochondria (Tom20), the early endosome (EEA1 and Rab5), or the exocytotic vesicles (Rab3 and 4) (Fig. 1A, B and S1). GFP signals in SH-SY5Y cells that stably expressed GFP-tagged wild-type ATP13A2 (GFP-WT) strongly colocalized with either of two lysosomal membrane proteins, Lamp2 (Fig. 1A and S1) or Lamp1 (data not shown). Furthermore, immunoelectron microscopy using ultrathin cryosections of GFP-WT SH-SY5Y cells confirmed that gold particles labeling GFP-WT (arrow head: 10 nm gold) and those labeling Lamp1 (arrow: 5 nm gold) co-localized on the lysosomal membrane (Fig. 1C). These data indicated that ATP13A2 is a resident protein of the lysosomal membrane.

Thus far, eight disease-associated mutations have been identified in the *ATP13A2* gene, including one that we described initially [3–8]. To determine whether the mutant proteins were mislocalized and whether any such mislocalization has etiological importance, we assessed the subcellular localization of five pathogenic protein variants (Fig. 2A). These mutants were each tagged with a V5 epitope and then transiently transfected into SH-SY5Y cells. To, first, characterize the subcellular distribution of KRS mutants, we separated cell homogenates by Percoll density gradient centrifugation. This Percoll gradient system separates dense lysosomes (near bottom) from lighter particles such as ER. We found that WT-V5 was mainly co-fractionated with lysosomal component (Lamp1 and cathepsin D; Fraction No. 13–16, Fig. 2B). However, an ATP13A2 variant that lacks exon 13 (1306 + 5G→A) but maintains the reading frame was co-fractionated not with lysosomal proteins but with GRP78 (Fraction No. 2–8, Fig. 2B): this finding indicated that the protein variant accumulated in the ER. Some other ATP13A2 pathogenic variants (F182L and G504R) also accumulated in the ER in a manner similar to the 1306 + 5G→A variant. In contrast, the other two pathogenic variants (T12M and G533R) were co-fractionated with lysosomal components, as was the WT protein. To, further, confirm the subcellular localization, we carried out double fluorescence immunocytochemistry of permeabilized SH-SY5Y cells by staining KRS mutants (V5), the ER marker (GRP78), the lysosomal marker (cathepsin D) and the mitochondria marker (Tom20). Along with immunoblotting of Percoll density gradient fractionation, immunofluorescence studies showed 1306 + 5G→A mutant, F182L and G504R colocalized with GRP78 and the other two variants (T12M and G533R) colocalized with cathepsin D as already reported [10–14] (Fig. 2C and S1). The expression levels of ATP13A2 mutant proteins that accumulated in the ER (F182L, G504R, and 1306 + 5G→A) were lower than that of the WT protein and MG132 inhibited degradation of the all ATP13A2 variants as well as that of the WT protein (Fig. 2D).

2.2. Stable knockdown of ATP13A2 induces cathepsin D deficiency and structures that resemble neuronal ceroid-lipofuscinosis deposits

To assess whether the loss of normal ATP13A2 functions has a causal role in PD pathogenesis, the expression of endogenous ATP13A2 was suppressed in SH-SY5Y cells by gene knockdown. By using antibodies that we generated (Fig. 3A), we showed that endogenous ATP13A2 protein levels in SH-SY5Y cells that stably expressed ATP13A2 shRNA (ATP13A2shRNA-1 or -2) were efficiently suppressed (Fig. 3B). Water soluble Tetrazolium salts (WST)-8 assay demonstrated that ATP13A2 knockdown caused a significant reduction of the cell growth in SH-SY5Y cells (Fig. 3B). Next, we determined the distribution and the morphology of lysosomes in SH-SY5Y cells subjected to ATP13A2 knockdown. Immunostaining of cathepsin D and Lamp2 indicated that ATP13A2 deficiency led to the assembly of lysosomes in the perinuclear region and decreased cathepsin D staining (Fig. S2). The protein amount of full length (52-kDa), immature (44-kDa) and mature (32-kDa) forms of cathepsin D of the cells expressing ATP13A2 shRNAs were all decreased together with the enzyme activity (Fig. 3C). To show the reduction of cathepsin D activity was indeed induced by the reduction of ATP13A2, not by the non-specific effect of shRNA, we generated shRNA-resistant species of ATP13A2. SH-SY5Y cells stably expressing ATP13A2 shRNAs that were transfected with shRNA resistant ATP13A2 showed comparable cathepsin D activity to the controls (Fig. S3A). The activity and amount of mature forms (25-kDa) of cathepsin B and L were also decreased in the knockdown cells line by ATP13A2 shRNA-1, but not shRNA-2, suggesting that the loss of ATP13A2 principally gives rise to the reduction of cathepsin D (Fig. 3C). Finally, analysis via transmission electron microscopy revealed that lysosome-like bodies became more numerous in ATP13A2 shRNAs expressing cells and that very immense high density structure appeared adjacent to the nucleus in these cells (Fig. 3D: a–h). High-magnification images revealed that the abnormal structures in these cells included fingerprint profiles-like structure (Fig. 3D: e), and these structures were very similar to the structure of the neurons in mice lacking cathepsin D [15]. The levels of LC3-II, autophagosome marker, in shRNA-1 transfected cells were increased (Fig. 3E) and p62 a substrate of autophagic degradation, was accumulated in both of the shRNA expressing lines (Fig. S3B), suggesting that an appearance of abnormal structure induced by ATP13A2 deficiency might be involved with impaired lysosomal proteolysis. Taken together, these findings indicated that loss of ATP13A2 led to lysosomal pathology and, more specifically, a reduction in cathepsin D activity.

2.3. Generation of an Atp13a2 mutant medaka fish

Next, we generated and evaluated medaka fish with an Atp13a2 mutation to investigate the mechanism of KRS/PARK9-associated neurodgeneration in vivo. The draft of the medaka genome contains only one identifiable ortholog of the human *ATP13A2* gene. We cloned the medaka *atp13a2* gene by RT-PCR and RACE, and it encoded a protein consisting of 1159 amino acids. The amino-acid sequence showed 51.3% homology to human ATP13A2 protein (Fig. S4A). To characterize medaka *atp13a2* expression, we used in situ hybridization to visualize medaka *atp13a2* mRNA. No signal was observed with the sense RNA probe. However, the anti-sense RNA probe resulted in diffuse signals in the gray matter of medaka brain (Fig. 4A). The telencephalon and diencephalon that contain the putative striatum and many dopaminergic neurons, respectively, were intensely labeled by the anti-sense probe. The optic tectum was also intensely labeled, but the hindbrain and spinal cord were scarcely labeled (Fig. 4A).

We then used TILLING (Targeting Induced Local Lesions In Genomes) method to generate an Atp13a2 mutant fish [16]. We

Please cite this article in press as: Matsui, H., et al. ATP13A2 deficiency induces a decrease in cathepsin D activity, fingerprint-like inclusion body formation, and selective degeneration of dopaminergic neurons. FEBS Lett. (2013), http://dx.doi.org/10.1016/j.febslet.2013.02.046

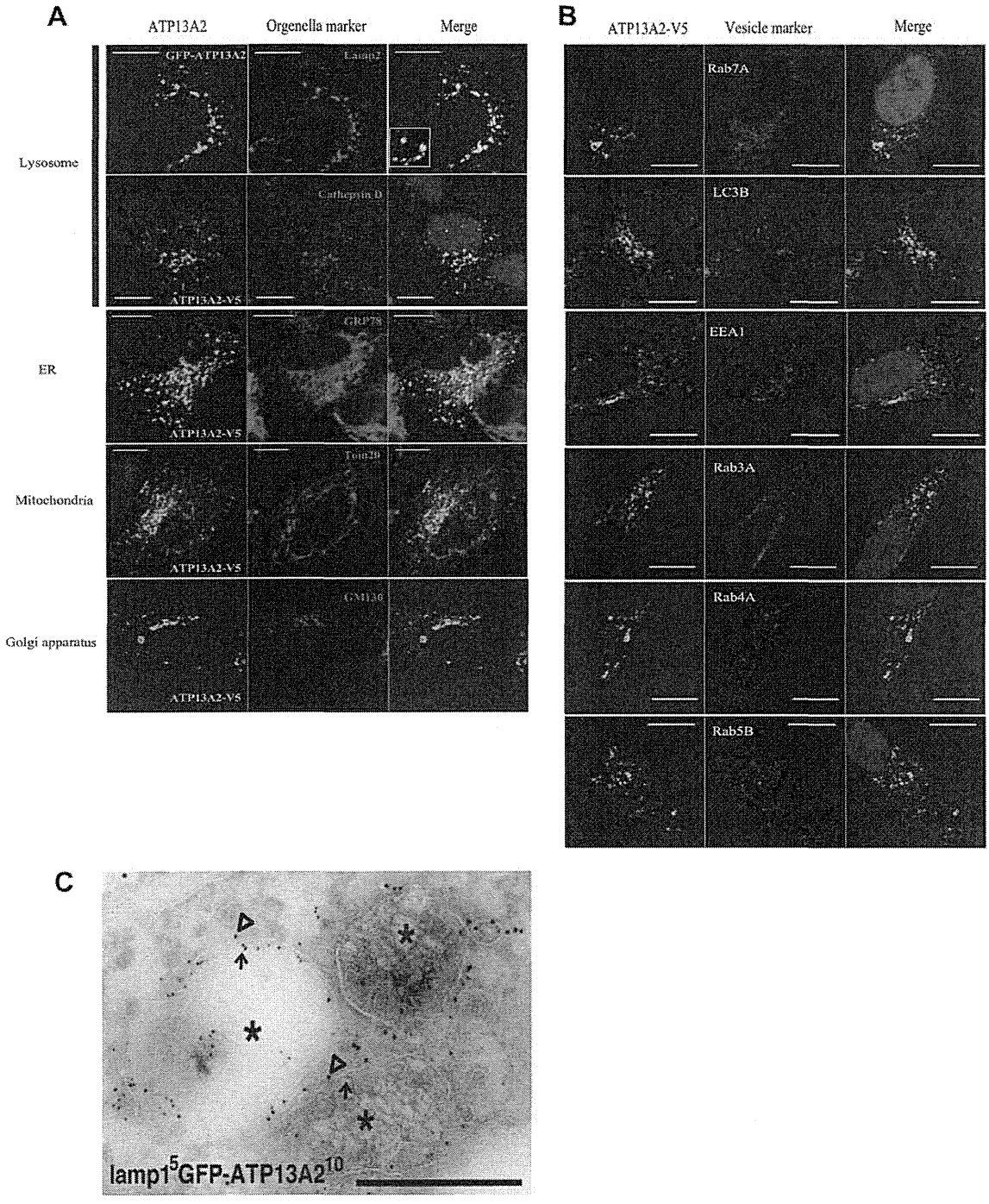

Fig. 1. Wild-type ATP13A2 localizes at lysosomal membranes. (A and B) WT-V5 and GFP-WT fusion proteins consistently co-localizes with Lamp2 and cathepsin D. Additionally, WT-V5 partially overlapped with GM130, Rab7 and LC3B. (Scale bar; 10 μm). (C) Immunoelectron microscopy using ultrathin cryosections. Double immunostaining of GFP-ATP13A2 (gold particles, 10 nm in diameter (open arrowheads)) and Lamp1 (gold particles, 5 nm in diameter (arrows)). Both types of immuno-gold label clearly localizes along the membranes around lysosomes (asterisks). (Scale bar; 0.5 μm).

sequenced the genomes of 5771 samples obtained from our ENU-mutagenized medaka library, and identified one mutation "IVS13, T-C, +2" that resulted in an aberrant splice donor site (Fig. 4B). The IVS13, T-C, +2 mutant from this strain was subjected to six sequential backcrosses to generate the mutant used in the following experiments. A cross between heterozygous "IVS13, T-C, +2" mutant pair resulted in wild-type fish (WT/WT), heterozygous mutants (WT/mt), and homozygous mutants (mt/mt) in Mendelian ratios. RT-PCR analysis revealed an abnormal splice variant in the WT/mt and mt/mt medaka (Fig. 4C), and the sequence of these PCR products indicated that exon 13 was skipped in the mutant mRNAs (Fig. 4D). Surprisingly, this abnormal splicing pattern was almost identical to that in the human KRS/PARK9 patient [3], in which the 111-bp exon 13 is skipped (Fig. S4B). Real-time PCR showed a marked reduction (17.8%) in the normal *atp13a2* mRNA in the mt/mt medaka brain (Fig. 4E). We therefore concluded that we had succeeded in identifying an Atp13a2 mutant in medaka, and this mutation was similar to a pathogenic KRS/PARK9 mutation in human.

Atp13a2 mutant medaka fish grew normally during early development without any obvious morphological abnormalities.

Please cite this article in press as: Matsui, H., et al. ATP13A2 deficiency induces a decrease in cathepsin D activity, fingerprint-like inclusion body formation, and selective degeneration of dopaminergic neurons. FEBS Lett. (2013), http://dx.doi.org/10.1016/j.febslet.2013.02.046

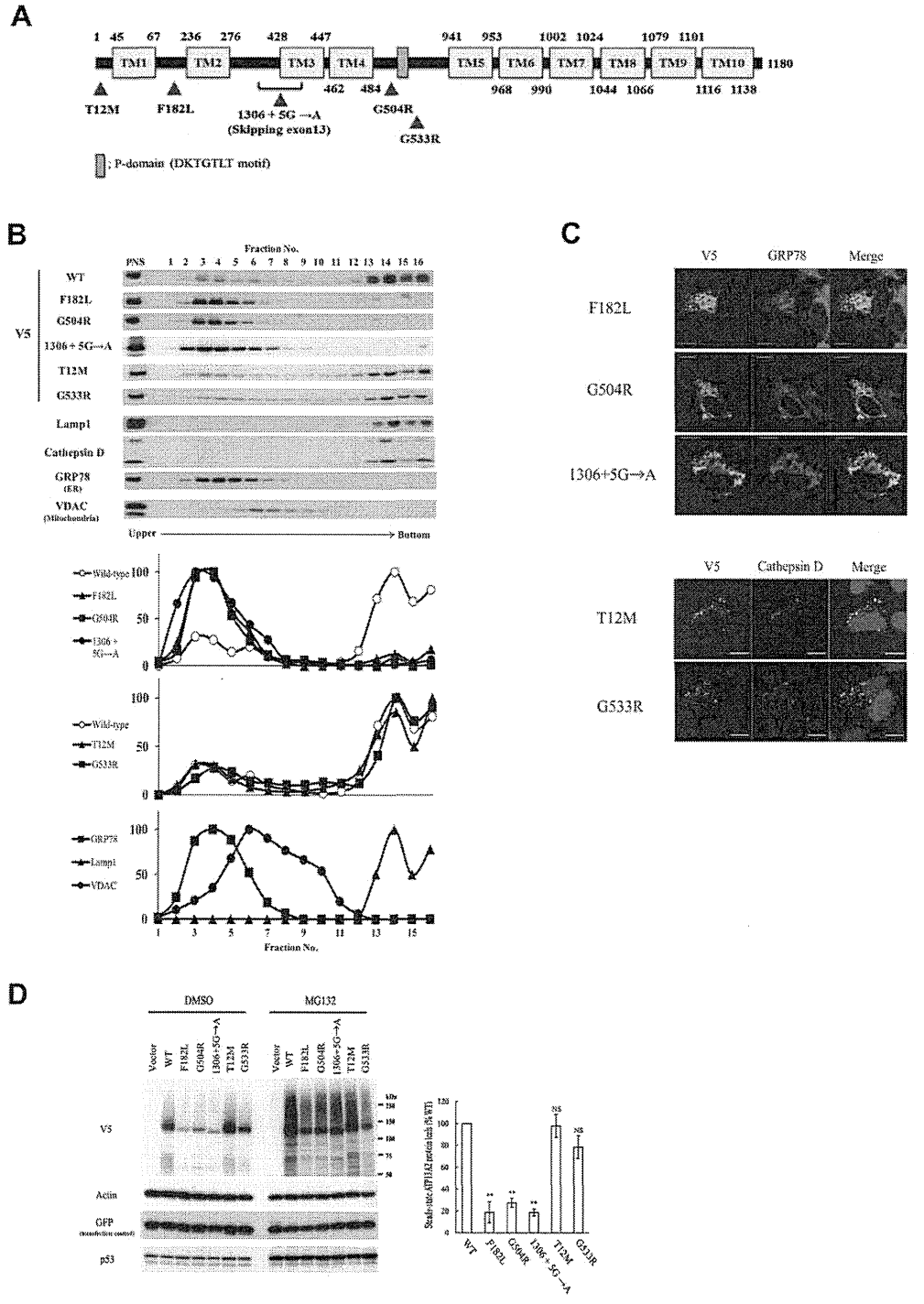

Fig. 2. Characterization of subcellular localization of KRS mutants. (A) Schematic diagram of disease-relevant mutants of ATP13A2 used in this study. (B) Percoll gradient fractionation of ATP13A2 protein. The graphs indicate densitometry of bands. This Percoll gradient system separates dense lysosomes (near bottom, Fraction 13–16) from lighter particles such as ER (Fraction 2–8). (C) Double immunofluorescence studies for KRS mutants. Colocalization of T12M or G533R with cathepsin D, a lysosomal protein, is observed. Other mutants localizes with GRP78, a resident ER chaperone protein. (D) Protein blot analysis of ATP13A2 WT and mutant V5-tagged constructs in transiently transfected SH-SY5Y cells. GFP was co-transfected with the ATP13A2s as a transfection control. The proteasome inhibitor MG132 (10 μM) stabilizes PARK9 mutants after 24 h. The antibody against p53, whose degradation is known to dependent to proteasome, is used as a control for MG132 treatment. Densitometry analysis indicates the steady state protein levels of each variant. Data are represented as percent of WT. Error bars, S.E.M. $n = 3$. $^{**}P < 0.01$ vs WT.

Remarkably, the mt/mt medaka fish showed a significant reduction of the life span relative to WT/WT and to WT/mt fish (Fig. 4F). The body weight of mt/mt fish was normal (Fig. 4G). We examined the internal organs including brains of the dead mt/mt fish, but we could not identify a specific reason for the shorter lifespan of mt/mt medaka fish. We next quantified spontaneous swimming movement in mt/mt medaka fish. At 4 months, mt/mt fish exhibited a mild locomotor increase with significant differences reported only in swimming duration whereas distance and velocity are normal. All the genotypes showed comparable movement at 12 months, irrespective of *atp13a2* genotype (Fig. 4H).

Collectively, we generated *atp13a2* mutant medaka fish carrying almost identical mutation to human KRS/PARK9 patient. The homozygous mutant fish grew normally, but relative to wild-type and heterozygous animals, these mutants exhibited more spontaneous swimming movement at 4 months and had a shorter life span.

Please cite this article in press as: Matsui, H., et al. ATP13A2 deficiency induces a decrease in cathepsin D activity, fingerprint-like inclusion body formation, and selective degeneration of dopaminergic neurons. FEBS Lett. (2013), http://dx.doi.org/10.1016/j.febslet.2013.02.046

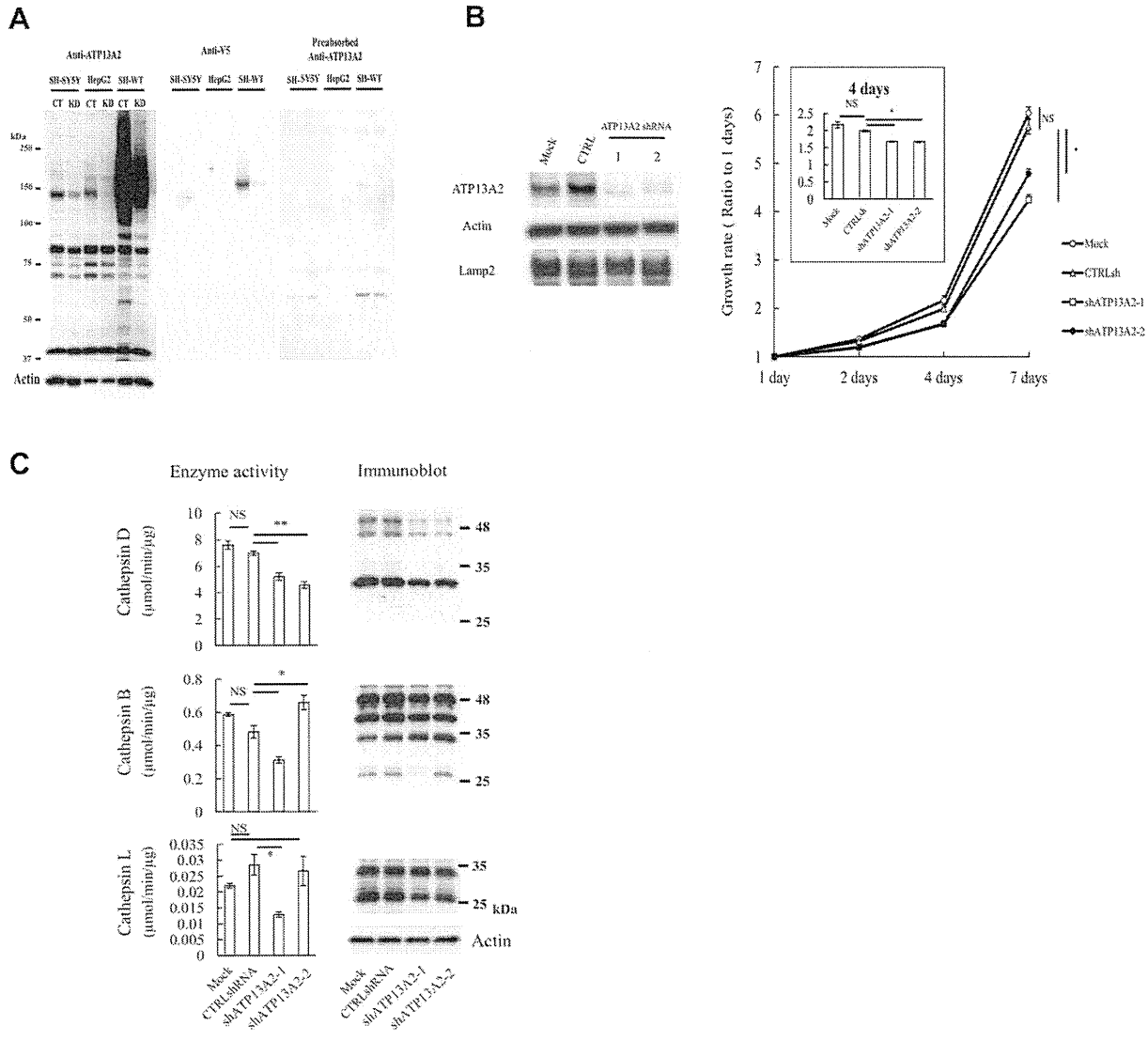

Fig. 3. Suppression of ATP13A2 leads to cathepsin D deficiency and accumulation of fingerprint-like structures in SH-SY5Y cells. (A) Immunoblotting with anti-ATP13A2 antibody (left panel), anti-V5 antibody (middle panel) and anti-ATP13A2 antibody (preabsorbed) (right panel) shows the ATP13A2 expression levels of SH-SY5Y cells, HepG2 cells and SH-SY5Y cells stably expressing WT (SH-WT). Cells are transfected with negative control (CT) or ATP13A2 siRNA (KD) for 72 h. (B) Immunoblotting using anti-ATP13A2 antibody and cell growth assay of SH-SY5Y cell lines stably expressing shRNA against human ATP13A2. The graph shows the growth rate of cells. Data are the means of triplicate experiments. Error bars, S.E.M. $^{*}P < 0.05$. (C) Measurement of cathepsin D, B and L activity and protein level in the extracts from ATP13A2-knockdown SH-SY5Y cells. Enzyme activity assays were performed in three independent experiments. Error bars, S.E.M. $^{*}P < 0.05$. $^{**}P < 0.01$. (D) Electron microscopic examination of SH-SY5Y cells that stably express shATP13A2-1 or shATP13A2-2. The diminished ATP13A2 expression induces lysosome-like bodies that contain granular deposits and fingerprint-like structure. Boxed areas (d) are shown enlarged in the left (e). (E) Evaluation of LC3 accumulation using anti-LC3B antibody in SH-SY5Y cell lines stably expressing shATP13A2 (each 3 clones). $^{**}P < 0.01$.

2.4. Neuropathology of *Atp13a2* mutant medaka fish

Selective and progressive loss of dopaminergic/noradrenergic cells constitutes the characteristic pathology of human PD patients. Having previously identified TH-positive (TH+) dopaminergic neurons and noradrenergic neurons in the medaka brain [17], we could examine histologically these TH+ neurons in the brain tissue of *atp13a2* mutants. At 4 months, the number of TH+ neurons did not differ significantly among mt/mt, mt/WT, and WT/WT fish. However at 8 and 12 months, the number of TH+ neurons in the middle diencephalon and the density of TH+ fibers in the telencephalon were lower in the mt/mt medaka than in mt/WT or in WT/WT fish (Fig. 5A). The mt/mt medaka fish at these stages also had fewer noradrenergic neurons in the medulla oblongata than did mt/WT or WT/WT fish (Fig. 5A). The reduction of TH+ neurons was not robust but age-dependent and progressive. Additionally, we examined tryptophan hydroxylase and serotonin levels via immunohistochemistry; neither the number of tryptophan hydroxylase positive neurons in the raphe nor the intensity of serotonin signals in the diencephalon differed significantly among all the genotypes (Fig. 5A). Although no TUNEL-positive dopaminergic neuron was observed in the WT/WT brains, a few TUNEL/TH double positive neurons were detected in the mt/mt brains (Fig. 5B). To exclude the possibility of developmental disorder of the dopaminergic neurons, we also counted the TH+ neurons in the middle diencephalon at 1 month. At this larval stage, mt/mt fish showed comparable number of dopaminergic neurons to WT/WT fish (Fig. S5) indicating the loss of dopaminergic neurons seen at 8 and 12 months was indeed late-onset phenotype. Next, we measured the amount of dopamine, noradrenaline, and serotonin in whole-brain samples from mutant fish at 4 and 12 months. The amount of dopamine in the brain samples from mt/mt medaka was comparable to that in the

Please cite this article in press as: Matsui, H., et al. ATP13A2 deficiency induces a decrease in cathepsin D activity, fingerprint-like inclusion body formation, and selective degeneration of dopaminergic neurons. FEBS Lett. (2013), http://dx.doi.org/10.1016/j.febslet.2013.02.046

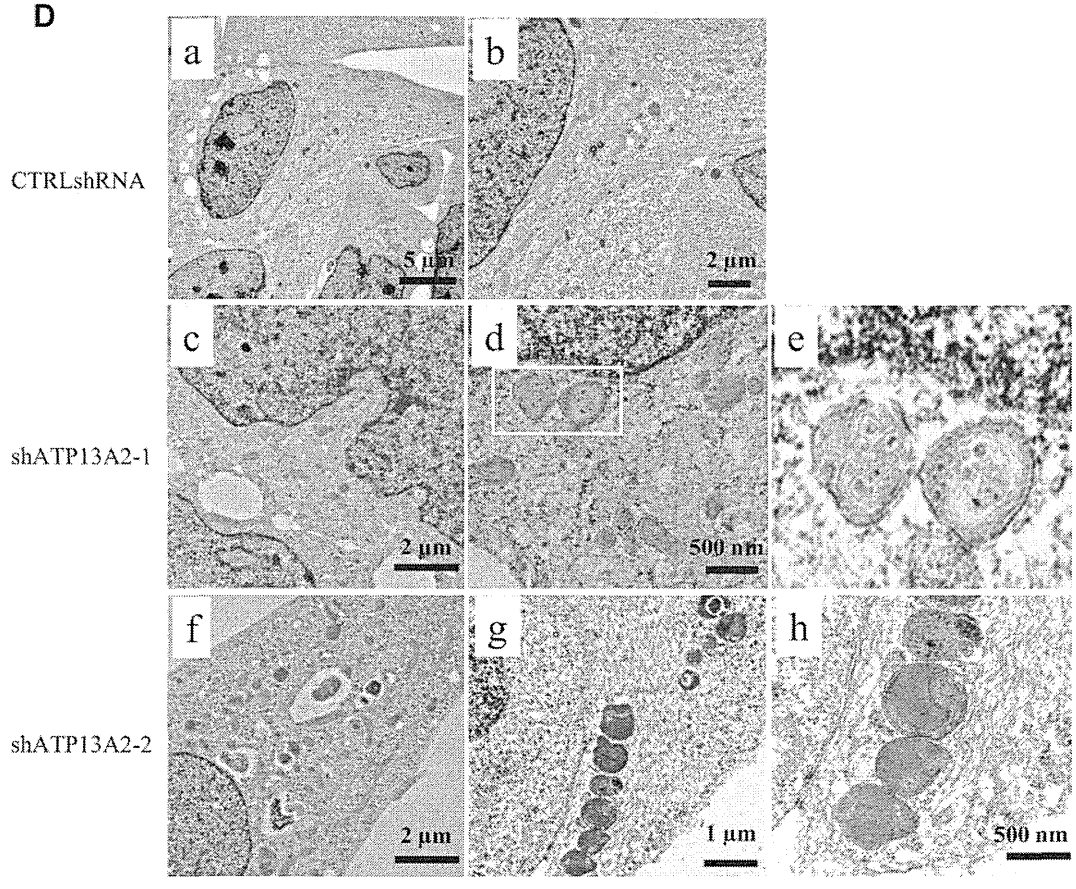

Fig. 3. (*continued*)

WT/WT or the WT/mt at 4 months, but lower than that in the WT/WT or the WT/mt at 12 months (Fig. 5C, upper). The noradrenaline in mt/mt medaka brain samples also tended to be lower at 12 months, but the differences were not statistically significant (Fig. 5C, middle). The amount of serotonin in whole-brain samples did not differ significantly among the genotypes (Fig. 5C, lower). Taken together, these findings indicated that *atp13a2* homozygous mutant medaka fish showed selective and progressive loss of dopaminergic/noradrenergic neurons, and such loss is a typical feature of human PD.

To examine in further detail the pathology associated with the *apt13a2* mutation, middle diencephalon samples from mt/mt, mt/WT, and WT/WT animals were analyzed via transmission electron microscopy as described previously [18]. Structures resembling fingerprints-profile, like those seen in ATP13A2-knockdown SH-SY5Y cells, were observed in thin sections taken from each mt/mt brain examined (Fig. 5D). However, these structures were not observed in the sections taken from WT/WT or WT/mt medaka brain samples. Fingerprint-profiles have been observed in cathepsin D-deficient mice [15] and in human patients with neuronal ceroid lipofuscinosis [19–21], and these structures are thought to indicate an autophagy/lysosome disorder. We used western blots to measure the amount of cathepsin D protein in brain tissue samples, and we found that mt/mt fish had less cathepsin D protein than did mt/WT or WT/WT fish (Fig. 5E and S6). We also showed that mt/mt medaka brain tissue, like the ATP13A2-knockdown cells, exhibited a significant reduction in cathepsin D activity (Fig. 5E). However, cathepsin K activity, cathepsin H activity, and proteasome activity were not affected by the *atp13a2* mutation (Fig. 5E), indicating the dysfunction of lysosomal enzymes was relatively specific to cathepsin D. Alpha-synuclein accumulation is one of the specific characters of idiopathic PD patients, Thus, we

Please cite this article in press as: Matsui, H., et al. ATP13A2 deficiency induces a decrease in cathepsin D activity, fingerprint-like inclusion body formation, and selective degeneration of dopaminergic neurons. FEBS Lett. (2013), http://dx.doi.org/10.1016/j.febslet.2013.02.046

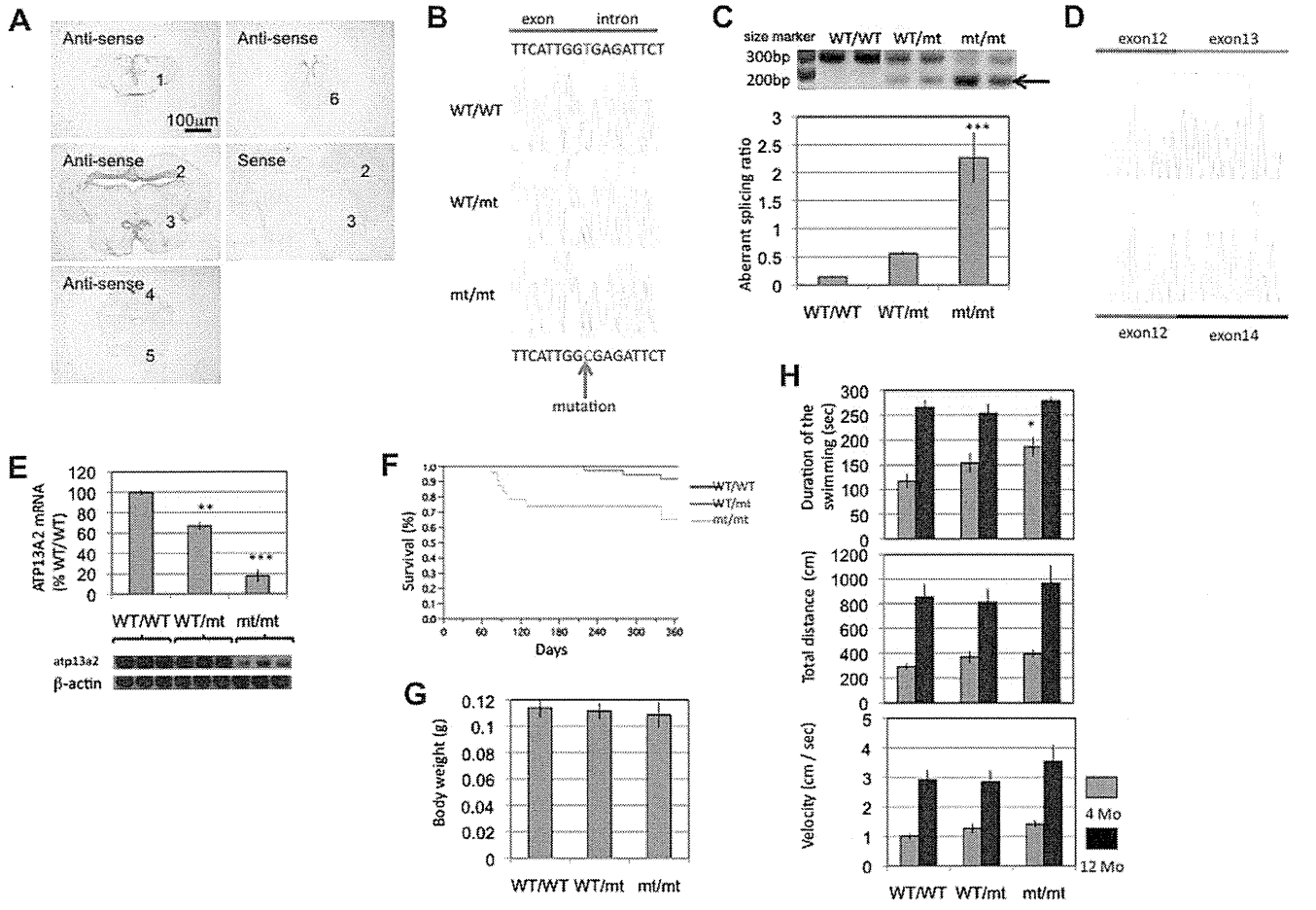

Fig. 4. Generation of Atp13a2 mutant medaka. (A) In situ hybridization of medaka *atp13a2* mRNA. Anti-sense signals and sense control of *Kyoto-Cab* medaka brain (12 months). 1: telencephalon, 2: optic tectum, 3: diencephalon, 4: cerebellum, 5: medulla oblongata, 6: spinal cord. (B) Sequence data for each genotype. A = green, T = red, G = black, and C = blue. The red arrow indicates the mutation site. This T to C mutation in the genomic sequence disrupts a splice donor site. (C) RT-PCR amplification of *atp13a2* mRNA from each genotype. WT/WT medaka show single band, whereas WT/mt and mt/mt medaka have an additional shorter band (arrow). bp: Base pairs. The graph indicates densitometric ratio of the shorter product/normal product. ***$P < 0.001$ vs. WT/WT and $P < 0.01$ vs. WT/mt. $n = 4$ for each genotype. Error bars, S.E.M. (D) Sequence of the PCR products. The upper band indicates the normal splicing product and the lower band is the abnormal splicing product. Exon 13 skipping occurrs in the Atp13a2 mutant medaka. (E) Real-time PCR of normal *atp13a2* mRNA. **: $P < 0.01$ vs. WT/WT, ***: $P < 0.001$ vs. WT/WT and WT/mt. $n = 3$ for each genotype. Error bars, S.E.M. (F) Survival curves of each genotype. The end point is the death of each medaka or day 365. The results show mild but significant shortening of the life span in mt/mt medaka ($P < 0.001$) ($n = 23$), relative to that in WT/WT ($n = 25$) or WT/mt ($n = 37$). Death before 1 month stage was not counted. (G) Body weight of Atp13a2 mutant medaka at 12 months. No significant differences were seen ($n = 20$ for each group). Error bars, S.E.M. (H) Duration of swimming, total swimming distance and swimming velocity during spontaneous swimming behavior of Atp13a2 mutant medaka ($n = 15$ for each group). *$P < 0.05$ vs. WT/WT. Error bars, S.E.M.

analyzed the alpha-synuclein status in our cell line and medaka models. However, we could not demonstrate consistent and significant differences between ATP13A2-deficient models and controls (Figs. S3 and S7), and these findings indicated that alpha-synuclein accumulation might not be the causative roles of KRS/PARK9.

In sum, *atp13a2* homozygous mutant medaka exhibited dopaminergic neurodegeneration, a deficiency of cathepsin D, and abnormal lysosome-related structures in the brain.

3. Discussion

Findings from previous studies clearly indicate that PARK gene products associate with each other via protein degradation pathways including the autophagy–lysosome system. Indeed, dysfunction of protein degradation has emerged as an important contributor to nigral neuronal death in PD. Presence of Lewy bodies is strong evidence of impaired protein degradation in PD. Lewy bodies consist of aggregated proteins, and alpha-synuclein is a major component of these structures [22]. Thus aggregation of alpha-synuclein has emerged as one of the most important processes in nigral degeneration in PD. Although soluble alpha-synuclein is degraded both during autophagy and by the proteasome, aggregated alpha-synuclein is degraded and cleared mainly via the autophagy–lysosome pathway [23]. Other PARK gene products, specifically Parkin and PINK1, work together to clear damaged mitochondria from cells via mitochondria-specific autophagy called mitophagy [24]. Furthermore, ATP13A2 mainly localizes to lysosomes, as we and other groups demonstrated [3,10–14,25]. Recently, mutations in the gene encoding glucocerebrosidase (GBA), a lysosomal enzyme, have been shown to be significant genetic risk factors for PD [26]. These observations indicate that lysosomal function is important for the maintenance of dopamine neurons, and they led us to investigate the function of ATP13A2 in the pathophysiology of KRS/PARK9.

ATP13A2 deficiency resulted in an abnormal aggregation of lysosomes at perinuclear site. Furthermore, these accumulated vesicles were enlarged, as previously reported [27]. Moreover, we found evidence of lysosomal dysfunction in that cathepsin D activity was, specifically, reduced in ATP13A2-knockdown cells. Cathepsin D is a ubiquitously expressed lysosomal protease that is involved in proteolytic degradation, cell invasion, and apoptosis. Cathepsin D deficiencies cause neuronal ceroid lipofuscinosis, a

Please cite this article in press as: Matsui, H., et al. ATP13A2 deficiency induces a decrease in cathepsin D activity, fingerprint-like inclusion body formation, and selective degeneration of dopaminergic neurons. FEBS Lett. (2013), http://dx.doi.org/10.1016/j.febslet.2013.02.046

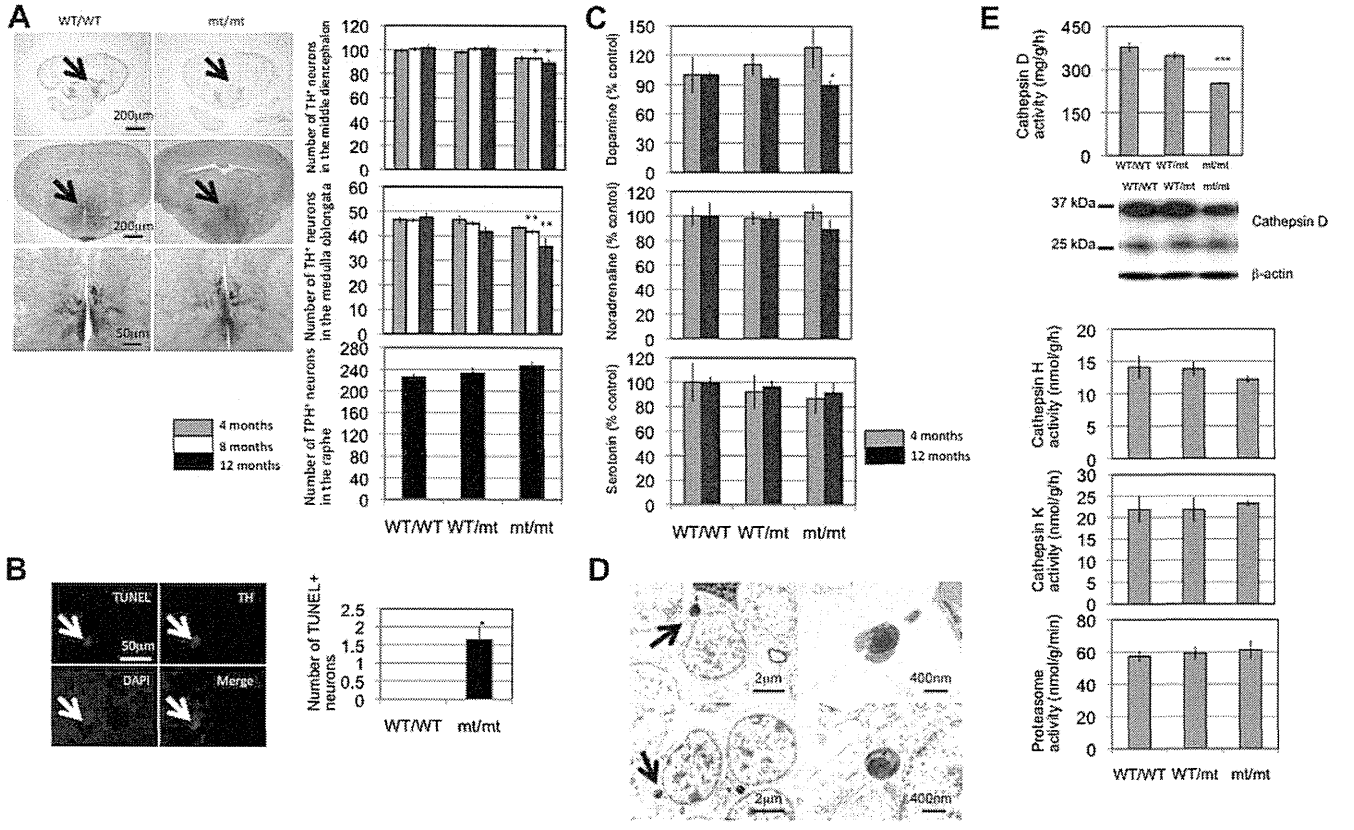

Fig. 5. Neuropathology of Atp13a2 mutant medaka. (A) Axial sections of telencephalon (upper) and middle diencephalon (middle and lower) of medaka brain at 12 months. Arrows indicate TH+ fibers and neurons. The lower figures are the enlarged image of middle figures. The graphs indicate the number of TH+ neurons in the middle diencephalon (upper) and medulla oblongata (middle) and the number of tryptophan-hydroxylase positive (TPH+) neurons in the raphe. $^{*}P < 0.05$ vs. WT/WT and WT/mt. $^{**}P < 0.01$ vs. WT/WT. ($n = 16$ for each group). Error bars, SEM. (B) TUNEL assay in medaka brain at 12 months. White arrow indicates one TUNEL/TH double positive neuron in the middle diencephalon of mt/mt fish. The graph shows the number of TH/TUNEL double positive neurons in the middle diencephalon ($n = 3$). $^{*}P < 0.05$ vs. WT/WT. (C) Amount of dopamine (upper), noradrenaline (middle), and serotonin (lower) in the brain of Atp13a2 mutant medaka. All values are expressed as a percentage of the amount (ng) per protein weight (mg) for WT/WT ($n = 8$ for each group). $^{*}P < 0.05$ vs. WT/WT. Error bars, S.E.M. (D) Fingerprint-like structures in Atp13a2 mutant medaka brain. Arrows indicate fingerprint-like structures in mt/mt brain. The right figures are the high magnification images of these structures. (E) Enzyme activity (Cathepsin D, H, K and proteasome activity) in the medaka brain. $^{***}P < 0.001$ vs. WT/T and WT/mt. Error bars, SEM. Image of a western blot shows cathepsin D protein in the medaka brain. Cross reactivity of the antibody against medaka cathepsin D is shown in the supplementary information (Fig. S5).

fatal neurogenerative disease in human and sheep [21,28–30]. Using electronmicroscopy, we also detected lysosome like body and granular deposits. Interestingly, we observed subcellular structures that resemble fingerprint-profile, and these structures resemble abnormal structures in the neurons of cathepsin D-deficient mice [15] and in human patients with neuronal ceroid lipofuscinosis [19–21] or with sphingolipidoses [31,32]. These results indicate that the primary cause of KRS/PARK9 is a lysosomal dysfunction and KRS/PARK9 could also be classified into a "lysosome disease".

We have recently used medaka fish to develop an animal model of PD [17,18,33,34]. Here, we found a mutation in our TILLING library that is almost identical to a PD-associated mutation in human patients. This medaka mutation results in the same abnormal splicing that is seen in the human patients with KRS/PARK9. Homozygous mutant fish exhibited selective loss of dopaminergic and noradrenergic neurons; this type of neuron loss is a pathology typically seen in human PD patients. Additionally, we found that tissues and cells in the brains from homozygous mutant medaka exhibited a specific reduction of cathepsin D protein and developed fingerprint-like subcellular structures. Both findings strongly indicate that the ATP13A2 mutation could lead to the dysfunction of lysosomes in medaka neurons.

Recently, Fonseca et al. injected Morpholinos against *atp13a2* into zebrafish embryo and showed that loss of Atp13a2 results in embryonic lethality [35]. As they also showed in zebrafish, *atp13a2* mRNA expressed not only in the brain but also in the entire body in medaka larvae (data not shown). This suggested that Atp13a2 is also important for some unknown function in other organs than the central nervous system. Our medaka model mimics the human mutation and showed pronounced reduction of *atp13a2* mRNA but not null expression. This might be helpful to study the long-term effect of Atp13a2 dysfunction.

As is the case of human patients with PD, cell death was specific to dopamine and noradrenaline neurons in our medaka model of KRS/ATP13A2. This cell-type specificity is also evident with our other medaka models of PD, including the models resulting from a lysosome inhibitor treatment [18,34]. The *atp13a2* mRNA, like other PD-related mRNAs, is expressed ubiquitously in the medaka brain [33]. Thus, the expression pattern of *atp13a2* could not explain the selective cell death in our model. Dopamine neurons contain toxic proteins derived from dopamine itself [36,37], and lysosomal function is essential in these neurons for preventing accumulation of the toxic proteins and other toxic metabolic products. Therefore, we speculate that dopamine neurons are especially vulnerable to lysosome dysfunction.

One negative finding is that mutant fish did not show slow locomotive movement, as do human PD patients. Based on our analysis, it seemed that the mutant fish swam the same amount, or more, than did control fish. In humans, loss of at least 80% of the dopaminergic neurons in substantia nigra seems necessary to evoke clear PD symptoms. The extent of the loss of dopaminergic

Please cite this article in press as: Matsui, H., et al. ATP13A2 deficiency induces a decrease in cathepsin D activity, fingerprint-like inclusion body formation, and selective degeneration of dopaminergic neurons. FEBS Lett. (2013), http://dx.doi.org/10.1016/j.febslet.2013.02.046

neurons in our medaka model might not be enough to evoke locomotive impairment. The mild increase of locomotion at 4 months seen in homozygous mutant might have a relation with the non-significant increase of dopamine at the same stage. Similar tentative increase of dopamine at younger stage is also observed in another PD model fish [33]. Such increased dopamine might harm the neurons, because the metabolism of dopamine is accompanied by the generation of oxidative radicals [38].

In conclusion, we demonstrated that reduction in ATP13A2 function in vitro or in vivo resulted in dysfunction of cathepsin D and the appearance of abnormal structures that are associated with lysosomal disorders. We used a teleost fish, medaka, to successfully generate an animal model suffered selective degeneration of dopaminergic neurons. Our findings indicate that lysosome-mediated autophagy may play a key role to protect dopaminergic neurons.

Acknowledgments

We wish to thank Kondoh Differentiation Signaling Project, JST, for permission to use the Kyoto-cab strain. We are grateful to Ai Tanigaki, Rie Hikawa and Junji Ezaki, who were very supportive of our experiments. We are also grateful to Satoshi Fukui, Mitsutaka Yoshida, Kaori Moriya, and Hidetake Kurihara for excellent assistance with our electron microscopy studies. This work was supported by JST-CREST. A part of this research was supported by a Grant-in-Aid for Young Scientists (B) (F. Sato) and a Grant-in-Aid for Scientific Research on Innovative Areas (Comprehensive Brain Science Network) (F. Sato) from the Ministry of Education, Science, Sports and Culture of Japan.

Appendix A. Supplementary data

Supplementary data associated with this article can be found, in the online version, at http://dx.doi.org/10.1016/j.febslet.2013.02.046.

References

Q3 [1] Gasser, T. (2007) Update on the genetics of Parkinson's disease. Mov. Disord. 22 (Suppl. 17), S343–S350.
[2] Najim al-Din, A.S., Wriekat, A., Mubaidin, A., Dasouki, M. and Hiari, M. (1994) Pallido-pyramidal degeneration, supranuclear upgaze paresis and dementia: Kufor-Rakeb syndrome. Acta Neurol. Scand. 89, 347–352.
[3] Ramirez, A., Heimbach, A., Gründemann, J., Stiller, B., Hampshire, D., Cid, L.P., Goebel, I., Mubaidin, A.F., Wriekat, A.L., Roeper, J., et al. (2006) Hereditary parkinsonism with dementia is caused by mutations in ATP13A2, encoding a lysosomal type 5 P-type ATPase. Nat. Genet. 38, 1184–1191.
[4] Di Fonzo, A., Chien, H.F., Socal, M., Giraudo, S., Tassorelli, C., Iliceto, G., Fabbrini, G., Marconi, R., Fincati, E., Abbruzzese, G., et al. (2007) ATP13A2 missense mutations in juvenile parkinsonism and young onset Parkinson disease. Neurology 68, 1557–1562.
[5] Ning, Y.P., Kanai, K., Tomiyama, H., Li, Y., Funayama, M., Yoshino, H., Sato, S., Asahina, M., Kuwabara, S., Takeda, A., et al. (2008) PARK9-linked parkinsonism in eastern Asia: mutation detection in ATP13A2 and clinical phenotype. Neurology 70, 1491–1493.
[6] Paisán-Ruiz, C., Guevara, R., Federoff, M., Hanagasi, H., Sina, F., Elahi, E., Schneider, S.A., Schwingenschuh, P., Bajaj, N., Emre, M., et al. (2010) Early-onset L-dopa-responsive parkinsonism with pyramidal signs due to ATP13A2, PLA2G6, FBXO7 and spatacsin mutations. Mov. Disord. 25, 1791–1800.
[7] Santoro, L., Breedveld, G.J., Manganelli, F., Iodice, R., Pisciotta, C., et al. (2011) Novel ATP13A2 (PARK9) homozygous mutation in a family with marked phenotype variability. Neurogenetics 12, 33–39.
[8] Crosiers, D., Ceulemans, B., Meeus, B., Nuytemans, K., Pals, P., Van Broeckhoven, C., Cras, P. and Theuns, J. (2011) Juvenile dystonia–parkinsonism and dementia caused by a novel ATP13A2 frame-shift mutation. Parkinsonism Relat. Disord. 17, 135–138.
[9] Lesage, S. and Brice, A. (2009) Parkinson's disease: from monogenic forms to genetic susceptibility factors. Hum. Mol. Genet. 18, R48–R59.
[10] Covy, J.P., Waxman, E.A. and Giasson, B.I. (2012) Characterization of cellular protective effects of ATP13A2/PARK9 expression and alterations resulting from pathogenic mutants. J. Neurosci. Res. 90, 2306–2316.
[11] Dehay, B., Ramirez, A., Martinez-Vicente, M., Perier, C., Canron, M.H., Doudnikoff, E., Vital, A., Vila, M., Klein, C. and Bezard, E.C. (2012) Loss of P-type ATPase ATP13A2/PARK9 function induces general lysosomal deficiency and leads to Parkinson disease neurodegeneration. Proc. Natl. Acad. Sci. USA 109, 9611–9616.
[12] Podhajska, A., Musso, A., Trancikova, A., Stafa, K., Moser, R., Sonnay, S., Glauser, L. and Moore, D.J. (2012) Common pathogenic effects of missense mutations in the P-type ATPase ATP13A2 (PARK9) associated with early-onset parkinsonism. PLoS ONE 7, e39942.
[13] Ramonet, D., Podhajska, A., Stafa, K., Sonnay, S., Trancikova, A., Tsika, E., Pletnikova, O., Troncoso, J.C., Glauser, L. and Moore, D.J. (2012) PARK9-associated ATP13A2 localizes to intracellular acidic vesicles and regulates cation homeostasis and neuronal integrity. Hum. Mol. Genet. 21, 1725–1743.
[14] Usenovic, M., Knight, A.L., Ray, A., Wong, V., Brown, K.R., Caldwell, G.A., Caldwell, K.A., Stagljar, I. and Krainc, D. (2012) Identification of novel ATP13A2 interactors and their role in α-synuclein misfolding and toxicity. Hum. Mol. Genet. 21, 3785–3794.
[15] Koike, M., Nakanishi, H., Saftig, P., Ezaki, J., Isahara, K., Ohsawa, Y., Schulz-Schaeffer, W., Watanabe, T., Waguri, S., Kametaka, S., et al. (2000) Cathepsin D deficiency induces lysosomal storage with ceroid lipofuscin in mouse CNS neurons. J. Neurosci. 20, 6898–6906.
[16] Taniguchi, Y., Takeda, S., Furutani-Seiki, M., Kamei, Y., Todo, T., Sasado, T., Deguchi, T., Kondoh, H., Mudde, J., Yamazoe, M., et al. (2006) Generation of medaka gene knockout models by target-selected mutagenesis. Genome Biol. 7, R116.
[17] Matsui, H., Taniguchi, Y., Inoue, H., Uemura, K., Takeda, S. and Takahashi, R. (2009) A chemical neurotoxin, MPTP induces Parkinson's disease like phenotype, movement disorders and persistent loss of dopamine neurons in medaka fish. Neurosci. Res. 65, 263–271.
[18] Matsui, H., Ito, H., Taniguchi, Y., Inoue, H., Takeda, S. and Takahashi, R. (2010) Proteasome inhibition in medaka brain induces the features of Parkinson's disease. J. Neurochem. 115, 178–187.
[19] Palmer, D.N., Fearnley, I.M., Walker, J.E., Hall, N.A., Lake, B.D., Wolfe, L.S., Haltia, M., Martinus, R.D. and Jolly, R.D. (1992) Mitochondrial ATP synthase subunit c storage in the ceroid-lipofuscinoses (Batten disease). Am. J. Med. Genet. 42, 561–567.
[20] Tsiakas, K., Steinfeld, R., Storch, S., Ezaki, J., Lukacs, Z., Kominami, E., Kohlschütter, A., Ullrich, K. and Braulke, T. (2004) Mutation of the glycosylated asparagine residue 286 in human CLN2 protein results in loss of enzymatic activity. Glycobiology 14, 1C–5C.
[21] Tyynelä, J., Palmer, D.N., Baumann, M. and Haltia, M. (1993) Storage of saposins A and D in infantile neuronal ceroid-lipofuscinosis. FEBS Lett. 330, 8–12.
[22] Spillantini, M.G., Schmidt, M.L., Lee, V.M., Trojanowski, J.Q., Jakes, R. and Goedert, M. (1997) Alpha-synuclein in Lewy bodies. Nature 388, 839–840.
[23] Webb, J.L., Ravikumar, B., Atkins, J., Skepper, J.N. and Rubinsztein, D.C. (2003) Alpha-synuclein is degraded by both autophagy and the proteasome. J. Biol. Chem. 278, 25009–25013.
[24] Narendra, D., Tanaka, A., Suen, D.F. and Youle, R.J. (2008) Parkin is recruited selectively to impaired mitochondria and promotes their autophagy. J. Cell Biol. 183, 795–803.
[25] Tan, J., Zhang, T., Jiang, L., Chi, J., Hu, D., Pan, Q., Wang, D. and Zhang, Z. (2011) Regulation of intracellular manganese homeostasis by Kufor-Rakeb syndrome-associated ATP13A2 protein. J. Biol. Chem. 286, 29654–29662.
[26] Sidransky, E., Nalls, M.A., Aasly, J.O., Aharon-Peretz, J., Annesi, G., Barbosa, E.R., Bar-Shira, A., Berg, D., Bras, J., Brice, A., et al. (2009) Multicenter analysis of glucocerebrosidase mutations in Parkinson's disease. N. Engl. J. Med. 361, 1651–1661.
[27] Usenovic, M., Tresse, E., Mazzulli, J.R., Taylor, J.P. and Krainc, D. (2012) Deficiency of ATP13A2 leads to lysosomal dysfunction, α-synuclein accumulation, and neurotoxicity. J. Neurosci. 32, 4240–4246.
[28] Siintola, E., Partanen, S., Strömme, P., Haapanen, A., Haltia, M., Maehlen, J., Lehesjoki, A.E. and Tyynelä, J. (2006) Cathepsin D deficiency underlies congenital human neuronal ceroid-lipofuscinosis. Brain 129, 1438–1445.
[29] Fritchie, K., Siintola, E., Armao, D., Lehesjoki, A.E., Marino, T., Powell, C., Tennison, M., Booker, J.M., Koch, S., Partanen, S., et al. (2009) Novel mutation and the first prenatal screening of cathepsin D deficiency (CLN10). Acta Neuropathol. 117, 201–208.
[30] Steinfeld, R., Reinhardt, K., Schreiber, K., Hillebrand, M., Kraetzner, R., Bruck, W., Saftig, P. and Gartner, J. (2006) Cathepsin D deficiency is associated with a human neurodegenerative disorder. Am. J. Hum. Genet. 78, 988–998.
[31] Jellinger, K., Anzil, A.P., Seemann, D. and Bernheimer, H. (1982) Adult GM2 gangliosidosis masquerading as slowly progressive muscular atrophy: motor neuron disease phenotype. Clin. Neuropathol. 1, 31–44.
[32] Idoate, M.A., Pardo-Mindan, F.J. and Gonzalez Alamillo, C. (1992) Fabry's disease without angiokeratomas showing unusual eccrine gland vacuolation. J. Pathol. 167, 65–68.
[33] Matsui, H., Taniguchi, Y., Inoue, H., Kobayashi, Y., Sakaki, Y., Toyoda, A., Uemura, K., Kobayashi, D., Takeda, S. and Takahashi, R. (2010) Loss of PINK1 in medaka fish (*Oryzias latipes*) causes late-onset decrease in spontaneous movement. Neurosci. Res. 66, 151–161.
[34] Matsui, H., Ito, H., Taniguchi, Y., Takeda, S. and Takahashi, R. (2010) Ammonium chloride and tunicamycin are novel toxins for dopaminergic neurons and induce Parkinson's disease-like phenotypes in medaka fish. J. Neurochem. 115, 1150–1160.

Please cite this article in press as: Matsui, H., et al. ATP13A2 deficiency induces a decrease in cathepsin D activity, fingerprint-like inclusion body formation, and selective degeneration of dopaminergic neurons. FEBS Lett. (2013), http://dx.doi.org/10.1016/j.febslet.2013.02.046

[35] Lopes da Fonseca, T., Correia, A., Hasselaar, W., van der Linde, H.C., Willemsen, R. and Outeiro, T.F. (2013) The zebrafish homologue of Parkinson's disease ATP13A2 is essential for embryonic survival. Brain Res. Bull. 90, 118–126.
[36] Barzilai, A., Daily, D., Zilkha-Falb, R., Ziv, I., Offen, D., Melamed, E. and Shirvan, A. (2003) The molecular mechanisms of dopamine toxicity. Adv. Neurol. 91, 73–82.
[37] Gandhi, S., Vaarmann, A., Yao, Z., Duchen, M.R., Wood, N.W. and Abramov, A.Y. (2012) Dopamine induced neurodegeneration in a PINK1 model of Parkinson's disease. PLoS ONE 7, e37564.
[38] Blum, D., Torch, S., Lambeng, N., Nissou, M., Benabid, A.L., Sadoul, R. and Verna, J.M. (2001) Molecular pathways involved in the neurotoxicity of 6-OHDA, dopamine and MPTP: contribution to the apoptotic theory in Parkinson's disease. Prog. Neurobiol. 65, 135–172.

Please cite this article in press as: Matsui, H., et al. ATP13A2 deficiency induces a decrease in cathepsin D activity, fingerprint-like inclusion body formation, and selective degeneration of dopaminergic neurons. FEBS Lett. (2013), http://dx.doi.org/10.1016/j.febslet.2013.02.046

Biosci. Biotechnol. Biochem., **77** (4), 729–735, 2013

Comparative Analysis of the Expression Patterns of UPR-Target Genes Caused by UPR-Inducing Compounds

Satoko SHINJO, Yuji MIZOTANI, Etsu TASHIRO,† and Masaya IMOTO

Department of Biosciences and Informatics, Faculty of Science and Technology, Keio University, 3-14-1 Hiyoshi, Kohoku-ku, Yokohama 223-8522, Japan

Received October 19, 2012; Accepted January 10, 2013; Online Publication, April 7, 2013
[doi:10.1271/bbb.120812]

Endoplasmic reticulum (ER) stress, due to an accumulation of unfolded proteins in the ER, leads to a process known as the unfolded protein response (UPR). Since the several compounds used to induce UPR have different modes of action, their mechanisms of protein accumulation are thought to be different, but it is unclear whether these compounds can upregulate UPR target genes with similar kinetics. Hence, we sought to compare the expression patterns of nine UPR target genes induced by seven UPR-inducing compounds. Hierarchical clustering analysis revealed that the expression patterns of the UPR target genes induced by the seven compounds were classified into two clusters; cluster A (thapsigargin, tunicamycin, 2-deoxyglucose, and dithiothreitol) and cluster B (brefeldin A, monensin, and eeyarestatin I). Thus, this study suggests the existence of at least two types of UPR target gene expression profiles, which depend on the mode of action of the compounds.

Key words: unfolded protein response (UPR); endoplasmic reticulum (ER) stress; UPR-inducing compound; profiling

The endoplasmic reticulum (ER) is the organelle in which newly synthesized transmembrane and secreted proteins are folded. Proteins that have undergone the steps of conformational maturation, including folding, glycosylation, and intra/intermolecular disulfide bond formation, can be transported to their destination *via* the Golgi apparatus, but if the proteins have failed to form with the proper conformation, they accumulate in the ER lumen, a condition referred to as ER stress. In order to restore homeostasis in the ER, the cells activate an unfolded protein response (UPR) *via* activation of three ER transmembrane proteins, referred to as ER stress sensors: activating transcription factor 6 (ATF6), inositol-requiring kinase 1 (IRE1), and protein kinase regulated by RNA-like ER kinase (PERK). This is followed by the activation of specific transcription factors: activated ATF6 for ATF6, XBP1 (x-box binding protein 1) for IRE1, and ATF4 (activating transcription factor 4) for PERK. These transcription factors eventually upregulate the expression of UPR target genes to execute four responses: (i) translational attenuation to limit further protein load at the ER; (ii) enhancement of the capacity of the protein folding system through upregulation of ER chaperones or folding enzymes such as glucose-regulated proteins 78 (GRP78, also known as BiP, immunoglobulin-binding protein) and 94 (GRP94), protein disulfide isomerase (PDI), and ER-localized DnaJ 4 (ERdj4); (iii) facilitation of ER-associated degradation (ERAD), which is accelerated by enhancer mannosidase alpha-like 1 (EDEM1); and, (iv) induction of cellular apoptosis, in which C/EBP homologous protein (CHOP) is thought to play an important role if the adaptive responses (i–iii) are insufficient to relieve ER stress (review in refs. 1 and 2).

In most studies, UPR is induced by treating *in vitro* cell models with compounds such as tunicamycin, thapsigargin, and dithiothreitol (DTT), which impair the *N*-linked glycosylation of proteins,[3,4] the Ca^{2+}-dependent chaperone *via* inhibition of ER Ca^{2+} ATPase,[5,6] and protein disulfide bond formation[7,8] respectively. Moreover, brefeldin A, an inhibitor of Golgi-specific brefeldin A resistance factor 1 (GBF1),[9,10] 2-deoxyglucose, an analog of glucose and an inhibitor of *N*-linked glycosylation,[11] and eeyarestatin I, an inhibitor of ERAD,[12] also have been reported to induce UPR.[10,13,14] Since these compounds have different modes of action, the mechanisms of protein accumulation in the ER induced by the various compounds are thought to be different, but it is unclear whether these compounds upregulate all UPR target genes by similar kinetics. Therefore, in order to address our question, we compared the time-course expression profiles of UPR-target genes after treatment with UPR-inducing compounds.

First we first selected six compounds commonly used as UPR inducers: 2-deoxyglucose, brefeldin A, DTT, eeyarestatin I, thapsigargin, and tunicamycin. Exploratory chemical screening indicated that monensin induced the expression of GRP78 and other eight UPR-target genes, so this was added as a prospective UPR inducer (see below). We measured the expression of nine UPR target genes, ATF4, CHOP, EDEM1,

† To whom correspondence should be addressed. Tel: +81-45-566-1793; Fax: +81-45-566-1557; E-mail: tashiro@bio.keio.ac.jp

Abbreviations: ATF4, activating transcription factor 4; ATF6, activating transcription factor 6; CHOP, C/EBP homologous protein; DTT, dithiothreitol; EDEM1, ER degradation enhancer mannosidase alpha-like 1; eIF2α, eukaryotic initiation factor 2 α; ER, endoplasmic reticulum; ERAD, ER-associated degradation; ERdj4, ER-localized DnaJ 4; GADD34, growth arrest- and DNA damage-inducible gene 34; GBF1, Golgi-specific brefeldin A resistance factor 1; GRP78, glucose-regulated protein 78; GRP94, glucose-regulated protein 94; IRE1, inositol-requiring kinase 1; $p58^{IPK}$, protein kinase inhibitor of 58 kDa; PDI, protein disulfide isomerase; PERK, protein kinase regulated by RNA-like ER kinase; RT-PCR, reverse transcription PCR; UPR, unfolded protein response; VSVG, vesicular stomatitis virus G; XBP1, x-box binding protein 1

ERdj4, growth arrest- and DNA damage-inducible gene (GADD) 34, GRP78, GRP94, protein kinase inhibitor of 58 kDa ($p58^{IPK}$), and PDI. GADD34 and $p58^{IPK}$ have been reported to act as feedback regulators of UPR.[15,16] The expression profiles of these genes appeared to show characteristic patterns among the compounds. Hierarchical clustering analysis based on the kinetics of the expression of UPR target genes revealed at least two UPR target gene expression profiles, which were dependent on the mode of action of the UPR-inducing compound.

Materials and Methods

Materials. Tunicamycin, 2-deoxyglucose, monensin, and mouse monoclonal anti-β-actin (AC-74) were purchased from Sigma Aldrich (St. Louis, MO). Brefeldin A and DTT were from Calbiochem (San Diego, CA) and Wako Pure Chemical Industries, (Osaka, Japan) respectively. Thapsigargin and eeyarestatin I were from Santa Cruz Biotechnology (Santa Cruz, CA). Mouse monoclonal anti-KDEL (10C3) was from ENZO Life Sciences (Farmingdale, NY). Rabbit polyclonal anti-eIF2α and anti-phospho eIF2α (Ser51) were from Cell Signaling Technology (Beverly, MA). Rabbit polyclonal anti-PERK was from Rockland (Gilbertsville, PA). Horseradish peroxidase-conjugated anti-mouse IgG secondary antibody was from GE Healthcare (Little Chalfont, UK).

Cell culture. Human epithelial adenocarcinoma cell line HeLa was cultured in Dulbecco's Modified Eagle's Medium (DMEM; Nissui, Tokyo) supplemented with 8% fetal bovine serum at 37 °C in a 5% CO_2–95% air atmosphere.

Western blotting. Western blotting was performed as described previously.[17] Cell pellets were lysed using an extraction buffer containing 150 mM NaCl, 2.5 mM EGTA, 1 mM EDTA, 1 mM DTT, 0.1% Tween-20, 10 mM β-glycerophosphate, 1 mM NaF, 0.1 mM Na_3VO_4, 10% glycerol, and 50 mM HEPES (pH 7.5). Lysates were separated by 7%–10% SDS–PAGE and then subjected to immunoblotting. This was followed by detection using the ECL Western blotting detection system (Millipore, Bedford, MA) and on LAS-1000 CCD camera (Fujifilm, Tokyo). The visualized bands were quantified using ImageJ software (http://rsb.info.nih.gov/ij/).

Real-time RT-PCR. Reverse transcription was carried out as described previously.[18] Total RNA was extracted from HeLa cells and reverse-transcribed. The synthesized cDNA was subjected to quantitative real-time RT-PCR using SYBR premix Ex Taq (Takara, Shiga, Japan), and was detected using Thermal Cycler Dice Real Time System II (Takara). Data were analyzed using the Smart Cycler software program (Multiplate RQ version 1.00; Takara) by the relative quantification method.

Real-time cycle conditions for ERdj4 were 2 min at 50 °C, followed by 10 min at 90 °C, and then 45 cycles, each cycle 95 °C for 30 s and 63 °C for 1 min. The conditions for GAPDH were 10 s at 95 °C and then 35 cycles, each of 95 °C for 3 s, 60 °C for 10 s, and 72 °C for 10 s. RT-PCR conditions for all the other genes were 10 s at 95 °C and then 40 cycles, each cycle 95 °C for 3 s, 60 °C for 10 s, and 72 °C for 15 s. The sequences of the primer sets are shown in Table S1 (see *Biosci. Biotechnol. Biochem.* Web site). The amount of total RNA present in each reaction was normalized using GAPDH as internal control. Data are averages of at least three separate experiments, and one outlier was omitted in each case by Dixon's Q-test at the 99% confidence level.[19]

RNA interference. siRNA double-stranded oligonucleotides designed to interfere with the expression of PERK (HSS190343; Life Technologies) with siRNA as negative control (12935-300; Life Technologies) were used. Transfection of siRNA was demonstrated using Lipofectamine 2000 (Life Technologies) following the manufacturer's instructions. Briefly, HeLa cells were transfected with OPTI-MEM (Life Technologies) including siRNA and Lipofectamine 2000. Twenty-four h after transfection, the cells were trypsinized and seeded into 6-well plates. After further 24 h, the cells were treated with monensin and subjected to Western blotting.

Data processing and hierarchical clustering. The data acquired were normalized among genes and named "UPR fingerprints of genes," or reordered by compound and named "UPR fingerprints of compounds." Pearson's correlation coefficients between the UPR fingerprints were calculated, and these were used to determine degrees of similarity. Hierarchical clustering by an average linkage method was done using R version 2.13.1. (http://www.R-project.org).

Trypan blue dye exclusion assay. Cell viability was evaluated by trypan blue dye exclusion assay, as described previously.[20]

Results

Effects of the six UPR-inducing compounds on cell viability and GRP78 and GRP94 protein expression

Our first investigation was to determine suitable concentrations of six compounds (2-deoxyglucose, brefeldin A, DTT, eeyarestatin I, thapsigargin, and tunicamycin) for induction of UPR. GRP78 and GRP94 are well-known UPR marker proteins. Since the anti-KDEL antibody recognizes the KDEL sequence, a very common ER retention signal, it mainly detected both GRP78 and GRP94. Hence, using the anti-KDEL antibody, protein expression of them was examined in HeLa cells after 24-h of treatment with each of the six compounds (Fig. 1). As shown in Fig. 1A, 2-deoxyglucose induced the expression of GRP78 in a dose-dependent manner, with an approximately 1.5-fold increase at 0.2 mM and a maximum increase at 2 mM, and neither dose affected cell viability. Similarly, brefeldin A, thapsigargin, and tunicamycin also increased the expression of GRP78 in a dose-dependent manner, with maximum increases at 50 ng/mL, 30 nM, and 10 μg/mL, and with moderate increases (approximately 1.5-fold) at 15 ng/mL, 1 nM, and 1 μg/mL respectively. These doses also failed to affect cell viability (Fig. 1B, E, and F). DTT and eeyarestatin I induced GRP78 expression, at 3 mM and 3 μm respectively (Fig. 1C and D). Additionally, each of the compounds, except for brefeldin A, induced the expression of GRP94 similarly to GRP78, but the intensities of GRP78 and GRP94 protein expression induced by the various compounds were different. Upon treatment by brefeldin A, the expression of GRP94 increased in a dose-dependent manner. It reached a maximum at 50 ng/mL and then declined. Thus, it is likely that the expression patterns and the intensities of GRP78 and GRP94 induction were different among the compounds. In this study, the concentrations sufficient to induce maximum and moderate levels of UPR were defined with reference to the expression of GRP78 as to protein level, as summarized in Table 1.

Measurement of the time-course expression of the mRNA levels of nine UPR-target genes

To compare the expression patterns of UPR-target genes induced by the six UPR-inducing compounds, first we measured the mRNA levels of GPR78. HeLa cells were treated with one of the six compounds at the concentrations indicated in Table 1 and the amount of GRP78 mRNA was measured by real-time reverse transcription PCR (RT-PCR). As shown in Fig. 2, all six compounds increased the amount of GRP78 mRNA.

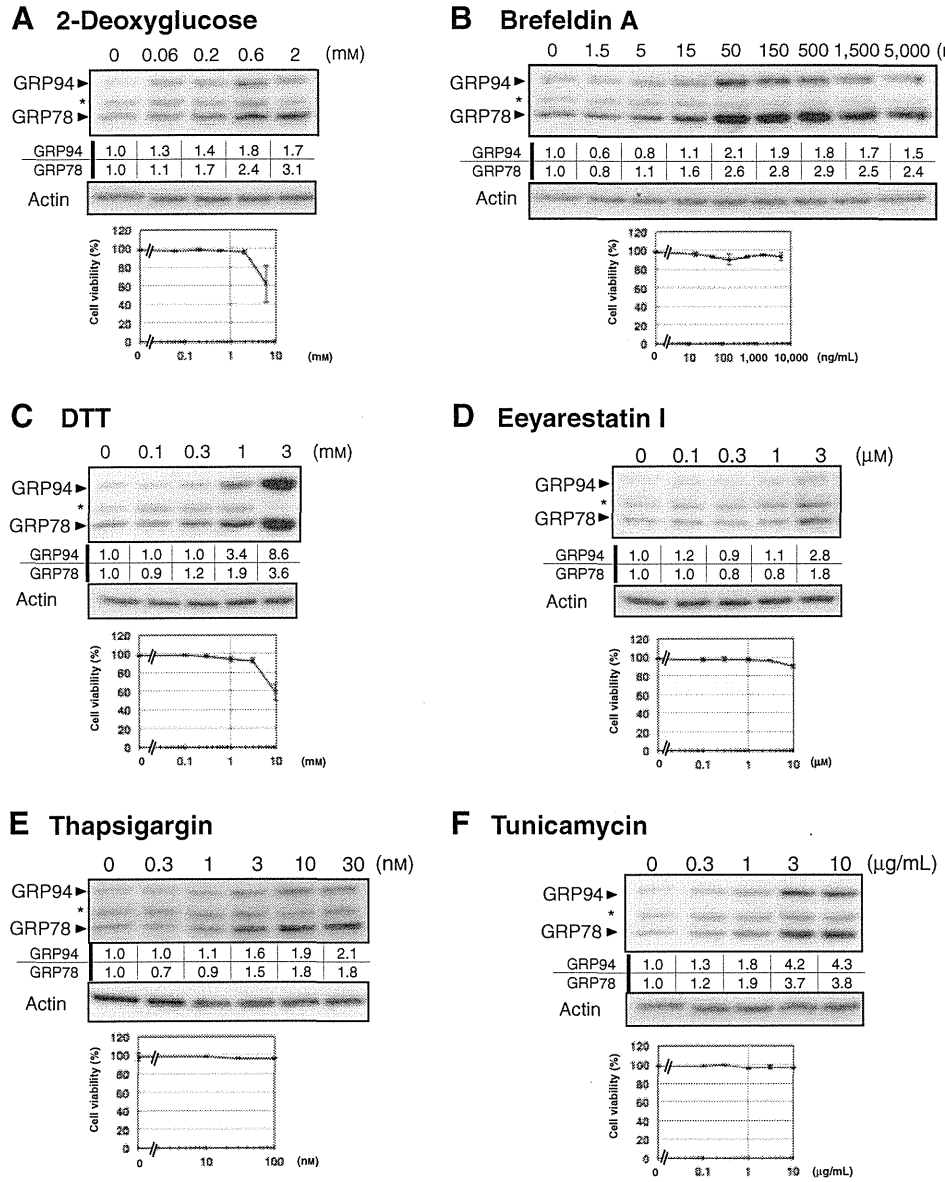

Fig. 1. UPR-Inducing Compounds Induced GRP78 Expression without Affecting Cell Viability.
Biological activity of six UPR-inducing compounds: 2-deoxyglucose (A), brefeldin A (B), DTT (C), eeyarestatin I (D), thapsigargin (E), and tunicamycin (F) (upper panel) HeLa cells were treated with the indicated concentrations of the compounds for 24 h. GRP78 and GRP94 were detected by immunoblotting with the anti-KDEL antibody. *Nonspecific band. The intensities of the bands of GRP78 and GRP94 were divided by that of β-actin and are indicated below the bands (lower panel) HeLa cells were treated with the indicated concentrations of the compounds for 24 h. Cell viability was assessed by trypan blue dye exclusion assay. Values are means of three independent determinations. Bars, SD.

Table 1. Concentrations of UPR-Inducing Compounds

Compound	Concentration	
	Inducing maximum GRP78 levels	Inducing moderate GRP78 levels
Thapsigargin	30 nM	1 nM
Tunicamycin	10 μg/mL	1 μg/mL
2-Deoxyglucose	2 mM	0.2 mM
DTT	3 mM	—
Brefeldin A	50 ng/mL, 5,000 ng/mL	15 ng/mL
Eeyarestatin I	3 μM	—

For instance, 30 nM thapsigargin increased it after 4-h of treatment, and it reached a plateau at an approximately 10-fold increase after 12-h of treatment. Two mM 2-deoxyglucose and 10 μg/mL tunicamycin also increased the amount of GRP78 mRNA, which peaked after approximately 12–16 h of treatment, resulting in 20- and 15-fold increases respectively, and then declined by the end of the 24-h treatment period (Fig. 2). When the cells were treated with 50 ng/mL of brefeldin A, the amount of GRP78 mRNA increased in a time-dependent manner for 24 h, showing an approximately 8-fold rise in expression (Fig. 2). Taken together, the time-course expression data for GRP78 mRNA appeared to show characteristic patterns among the six compounds.

Moreover, there were similar expression patterns for GRP78 mRNA when the HeLa cells were treated with 15 ng/mL, 50 ng/mL, or 5,000 ng/mL of brefeldin A. Furthermore, when the cells were treated with 0.2 mM and 2 mM of 2-deoxyglucose or 1 nM and 30 nM of thapsigargin, the expression patterns of GRP78 mRNA were also similar. In addition, 1 μg/mL of tunicamycin showed a slightly delayed expression pattern for GRP78 mRNA as compared to 10 μg/mL tunicamycin. Overall,

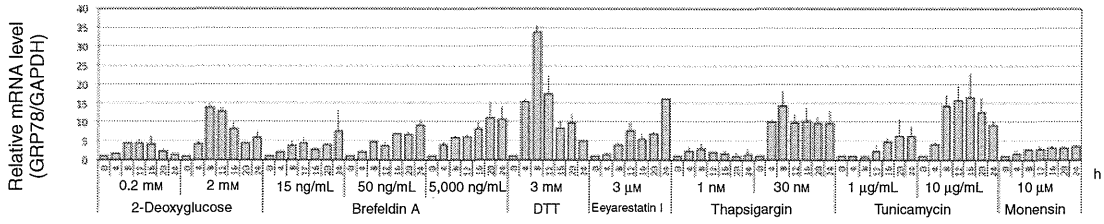

Fig. 2. UPR-Inducing Compounds Increased the Amount of GRP78 mRNA in the HeLa Cells.
HeLa cells were treated with UPR-inducing compounds at the indicated concentrations for 4–24 h. The relative mRNA levels of GRP78 were quantified by real-time RT-PCR. All values were normalized using GAPDH as internal control. Values are means of three independent determinations. Bars, SD.

the differences in the concentrations of the compounds did not have any notable effect on the expression patterns of GRP78 mRNA.

We further measured the changes in the amount of mRNA of an additional eight UPR target genes, ATF4, CHOP, EDEM1, ERdj4, GADD34, GRP94, PDI, and p58^{IPK}, when the cells were treated with each of the six compounds. As shown in Supplemental Fig. 1, all the compounds increased the amounts of the eight UPR target gene mRNA, at the concentrations indicated in Table 1.

Monensin upregulated UPR target genes

An in-house chemical library, which included commercially available compounds as well as compounds of microbial origin in our laboratory, was screened for additional potential UPR-inducing compounds. It was found that monensin, a compound first isolated from *Streptomyces cinnamonensis* and known as a Na^+ ionophore,[21] increased the amount of GRP78 at protein level with 10 μM treatment (Fig. 3A) without affecting cell viability (Fig. 3B). Monensin also increased the amount of GRP78 mRNA slightly at 4–24 h of treatment (Fig. 2), as well as the other eight UPR target genes of interest (Fig. S1). Furthermore, it induced phosphorylation of eIF2α, a well-known substrate of PERK[22] (Fig. 3C). Since four kinases (PERK, PKR, HRI, and GCN2) are known to phosphorylate eIF2α, we examined to determine whether monensin-induced phosphorylation of eIF2α occurs through PERK activation. As shown in Fig. 3C, monensin-induced phosphorylation of eIF2α was impaired in siPERK-transfected HeLa cells, in which successful knockdown of PERK was confirmed by immunoblotting (Fig. 3C), suggesting that monensin activated PERK. Thus, it appears that monensin induced UPR, and hence it was used in the remaining experiments in our study.

Clustering of compounds based on the expression profiles of the UPR target genes

It was observed that the kinetics of UPR target gene expression showed characteristic patterns among the 12 experimental conditions tested (seven compounds, some with multiple concentrations). The data acquired were analyzed by hierarchical clustering with the aim of classifying the expression profiles of the UPR target genes. The real-time RT-PCR data for each UPR target gene obtained under the 12 experimental conditions were normalized to acquire UPR fingerprints of genes. Furthermore, the normalized data were reordered by condition in order to acquire UPR fingerprints of

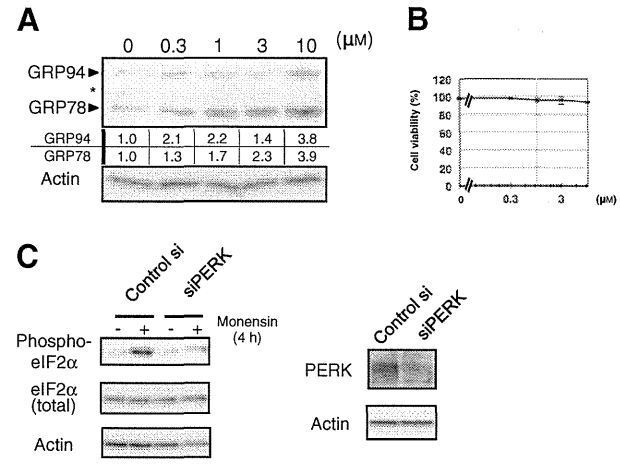

Fig. 3. Monensin Induced UPR.
The biological activity of monensin. (A) HeLa cells were treated with the indicated concentrations of monensin for 24 h. GRP78 and GRP94 were detected by immunoblotting with anti-KDEL antibodies. *Nonspecific band. The band intensities of GRP78 and GRP94 were divided by that of β-actin, and are indicated below the bands. (B) HeLa cells were treated with the indicated concentrations of monensin for 24 h. Cell viability was assessed by trypan blue dye exclusion assay. Values are means of three independent determinations. Bars, SD. (C) Control or PERK siRNA-transfected HeLa cells were treated with 10 μM monensin for 4 h. Total eIF2α and phospho-eIF2α were detected by immunoblotting. Successful knockdown of PERK by siRNA was confirmed by immunoblotting with anti-PERK antibody. β-Actin was immunoblotted as loading control.

compounds (Fig. 4). Each type of fingerprint was analyzed by hierarchical clustering using Pearson's correlation coefficient as a similarity and average-linkage method. As a result of clustering analysis of the compounds, as shown on the left side of Fig. 5, the 12 conditions were divided into two groups: cluster A and cluster B. Cluster A contained thapsigargin, tunicamycin, 2-deoxyglucose, and DTT, and cluster B contained brefeldin A, monensin, and eeyarestatin I. When thapsigargin, tunicamycin, 2-deoxyglucose, or brefeldin A was used at different concentrations, the expression patterns of the UPR target genes were still to be classified in the same cluster. Furthermore, as a result of clustering analysis of the genes, as shown at the top of Fig. 5, nine genes were classifiable into two groups: cluster I and cluster II (Fig. 5). Cluster I contained GRP78, ERdj4, EDEM1, p58^{IPK}, and GRP94, and cluster II contained GADD34, CHOP, PDI, and ATF4. Based on two-way clustering analysis, a heat map displayed the expression data for each gene under each condition by reordering of the data by rows and columns

(Fig. 5), indicated that the expression intensity of cluster I genes in the fingerprints of cluster A was higher than in cluster B; conversely, the expression intensity of cluster II genes in the fingerprints of cluster A was lower than in cluster B.

Discussion

In this study, by hierarchical clustering analysis, the expression patterns of UPR target genes induced by seven compounds were classified into two clusters.

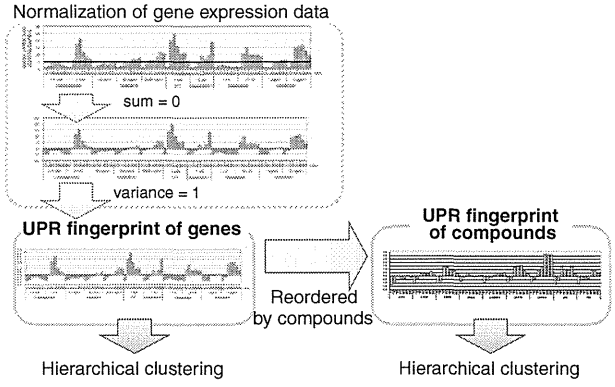

Fig. 4. Schematic Illustration of Method of Data Analysis.
The relative mRNA levels of the genes were normalized by subtracting the average value from the result at each time point and dividing by the standard derivative. A UPR fingerprint of genes was obtained. We created a separate UPR fingerprint of compounds by reordering the data compound-by-compound. Similarities between the two UPR fingerprints (Pearson's correlation coefficient) were calculated and analyzed by hierarchical clustering.

When cells were treated with thapsigargin, tunicamycin, 2-deoxyglucose, or brefeldin A at different concentrations, the expression patterns of the UPR-target genes were grouped into the same cluster (Fig. 5). This suggests that this grouping is due to the difference in the modes of action of the compounds, rather than their concentrations. The compounds comprising cluster A, thapsigargin, tunicamycin, 2-deoxyglucose, and DTT, showed a distinct mode of action, but they have been reported to inhibit the conformational maturation of proteins in the ER,[4,23–26] as described above in the introduction, leading to an accumulation of incorrectly folded proteins in the ER. On the other hand, among the compounds in cluster B, brefeldin A has been reported to accumulate correctly folded conformation of the vesicular stomatitis virus G (VSVG) protein, as judged by detection by the I14 antibody, which recognizes only the native or correctly folded conformation of the VSVG protein.[27,28] Thus, it is likely that the compounds in cluster B induced the expression of UPR target genes by accumulation of excess amounts of correctly folded proteins rather than incorrectly folded proteins in the ER. If this is the case, the difference in the expression patterns of UPR target genes as between cluster A and cluster B are related to the folding status of the accumulated proteins in the ER caused by the compounds in cluster A and cluster B. Eeyarestatin I and monensin were classified into cluster B, with the expectation that eeyarestatin I and monensin can accumulate excess amounts of correctly folded proteins in the ER. Indeed, eeyarestatin I has been reported to accumulate properly folded proteins as a consequence of

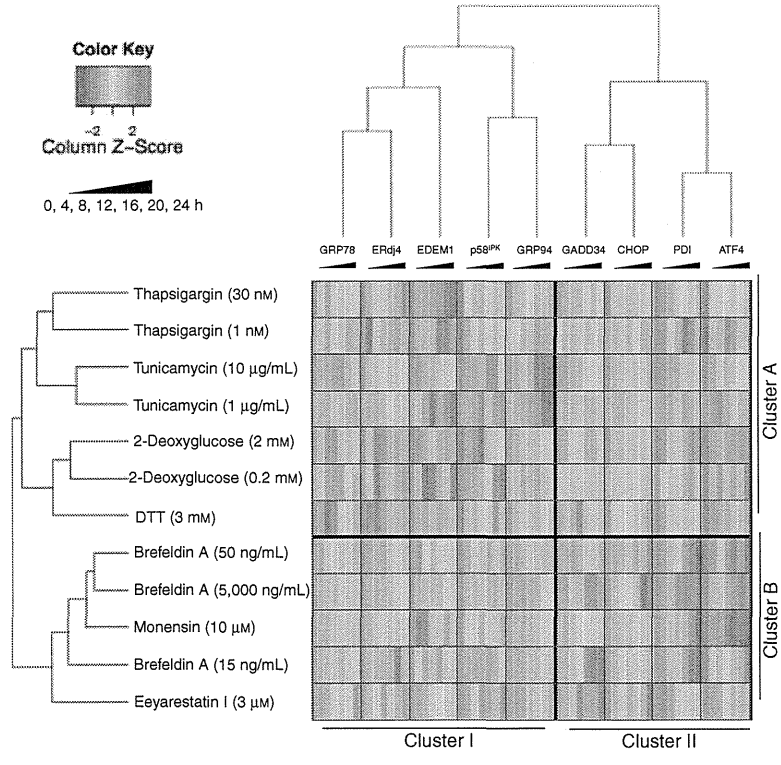

Fig. 5. Two-Dimensional Clustering Analysis of Genes and UPR-Inducing Compounds on the Basis of Pearson's Correlation Coefficients.
UPR fingerprints were analyzed by hierarchical cluster analysis. Dataset of 12 conditions and of nine genes were clustered by the average-linkage method using Pearson's correlation coefficients. Rows indicate seven different small molecular compounds (some with multiple concentrations; therefore 12 conditions). Columns indicate the nine UPR target genes, including the seven different time points. The heat map shows a gradient color scale from green, indicating the score in UPR fingerprint of compounds negative, to red, indicating the score positive, interpolated over gray for the score zero. The seven compounds and the nine genes were clustered into two groups, respectively.